

**HYDROGEN STORAGE IMPROVEMENT OF  
Ti-Zr-Ni-Mg BASED QUASICRYSTAL BY  
MECHANICAL ALLOYING PROCESS**



**Nitirut Phongsirimethi**

**A Thesis Submitted in Partial Fulfillment of the Requirements  
for the Degree of Master of Engineering in  
Mechanical and Process System Engineering  
Suranaree University of Technology  
Academic Year 2019**

การปรับปรุงการกัดเก็บไฮโดรเจนของควอสิคริสตัลชนิด Ti-Zr-Ni-Mg  
โดยกระบวนการผสมเชิงกล



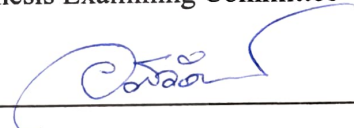
นายนิธิรจน์ พงศ์สิริเมธี

วิทยานิพนธ์นี้เป็นส่วนหนึ่งของการศึกษาตามหลักสูตรปริญญาวิศวกรรมศาสตรมหาบัณฑิต  
สาขาวิชาวิศวกรรมเครื่องกลและระบบกระบวนการ  
มหาวิทยาลัยเทคโนโลยีสุรนารี  
ปีการศึกษา 2562

# **HYDROGEN STORAGE IMPROVEMENT OF Ti-Zr-Ni-Mg BASED QUASICRYSTAL BY MECHANICAL ALLOYING PROCESS**

Suranaree University of Technology has approved this thesis submitted in partial fulfillment of the requirements for a Master's Degree.

Thesis Examining Committee

  
\_\_\_\_\_  
(Assoc. Prof. Dr. Apiwat Muttamara)

Chairperson

  
\_\_\_\_\_  
(Dr. Jittima Varagul)

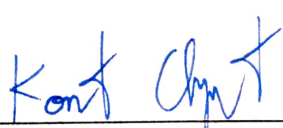
Member (Thesis Advisor)

  
\_\_\_\_\_  
(Asst. Prof. Dr. Wanwanut Boongsod)

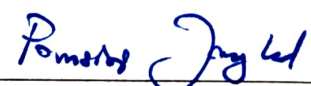
Member

  
\_\_\_\_\_  
(Dr. Somsak Siwadamrongpong)

Member

  
\_\_\_\_\_  
(Assoc. Prof. Ft. Lt. Dr. Kontorn Chamniprasart)

Vice Rector for Academic Affairs  
and Internationalization

  
\_\_\_\_\_  
(Assoc. Prof. Dr. Pornsiri Jongkol)

Dean of Institute of Engineering

นิธรุจน์ พงศ์ศิริเมธี : การปรับปรุงการกักเก็บไฮโดรเจนของควอสิคริสตัลชนิด Ti-Zr-Ni-Mg โดยกระบวนการผสมเชิงกล (HYDROGEN STORAGE IMPROVEMENT OF Ti-Zr-Ni-Mg BASED QUASICRYSTAL BY MECHANICAL ALLOYING PROCESS)  
อาจารย์ที่ปรึกษา : อาจารย์ ดร. จิตติมา วระกุล, 55 หน้า.

งานวิจัยนี้มุ่งเน้นไปที่การศึกษาการปรับปรุงความสามารถวัสดุที่ใช้ในการกักเก็บแก๊สไฮโดรเจน ซึ่งเป็นทางเลือกของพลังงานทดแทนที่มีความน่าสนใจเป็นอย่างมากเนื่องจากมีคุณสมบัติที่เหมาะสมหลายประการคือ เป็นมิตรต่อสิ่งแวดล้อม ให้พลังงานที่สูง และมีปริมาณมากบนโลก อย่างไรก็ตามการกักเก็บไฮโดรเจนเป็นเรื่องที่ทำหายเป็นอย่างมากเนื่องจากต้องคำนึงถึงในด้านความปลอดภัย ปริมาณในการกักเก็บ และวิธีการกักเก็บที่มีประสิทธิภาพ ในปัจจุบันมีนักวิจัยหลายท่านคิดค้นวิธีการและเทคโนโลยีเพื่อใช้กักเก็บไฮโดรเจน ซึ่งหนึ่งในวิธีที่มีความน่าสนใจคือวิธีการกักเก็บไฮโดรเจนโดยใช้วัสดุ

มีการรายงานว่า ควอสิคริสตัลกลุ่มโลหะผสมไทเทเนียม เซอร์โคเนียม และนิกเกิล เป็นองค์ประกอบ เป็นวัสดุที่ดีสำหรับการกักเก็บไฮโดรเจนเนื่องจากจำนวนช่องว่างระหว่างอะตอมที่มีมากถึง 140 ช่องว่าง ซึ่งมีมากกว่าผลึกแบบอื่นๆ นอกจากนี้ วัสดุแมกนีเซียมก็เป็นอีกหนึ่งวัสดุที่มีความสำคัญและเป็นที่น่าสนใจสำหรับการกักเก็บไฮโดรเจน แต่วัสดุแมกนีเซียมมีค่าเอนทัลปีและอุณหภูมิจากการดูดซับไฮโดรเจนค่อนข้างสูง

ในงานวิจัยนี้จะนำวัสดุทั้งสองชนิดที่ได้กล่าวมาคือ ควอสิคริสตัลและแมกนีเซียมผสมกันโดยวิธีการทางกลด้วยส่วนผสม  $Ti_{45-x}Zr_{38}Ni_{17}Mg_x$ ;  $x=2, 4$  โดยการบดผสมจะดำเนินการภายใต้ 2 เงื่อนไขคือ (1) ความเร็วรอบในการหมุน 600 รอบต่อนาที ใช้เวลาในการบด 20 ชั่วโมง และ (2) ความเร็วรอบในการหมุน 630 รอบต่อนาที ใช้เวลาในการบด 30 ชั่วโมง การทดสอบกักเก็บไฮโดรเจนจะใช้วิธีการกักเก็บโดยใช้ไฮโดรเจนแบบแก๊สด้วยวิธีการ pressure composition isotherm (PCT) จากการทดสอบพบว่าค่าการกักเก็บของไฮโดรเจนโดยเทียบอัตราส่วนระหว่างมวลของไฮโดรเจนและวัสดุกักเก็บ (H/M) ได้ค่าสูงสุดคือส่วนผสม  $Ti_{43}Zr_{38}Ni_{17}Mg_2$  เงื่อนไขที่ 1 ความเร็วรอบในการหมุน 600 รอบต่อนาที ใช้เวลาในการบด 20 ชั่วโมง โดยมีค่า H/M เท่ากับ 1.99 และสำหรับส่วนผสมเดียวกันใช้เงื่อนไขที่ 2 มีค่า H/M เท่ากับ 1.58

NITIRUT PHONGSIRIMETHI : HYDROGEN STORAGE IMPROVEMENT  
OF Ti-Zr-Ni-Mg BASED QUASICRYSTAL BY MECHANICAL  
ALLOYING PROCESS THESIS ADVISOR : JITTIMA VARAGUL, Ph.D.,  
55 PP.

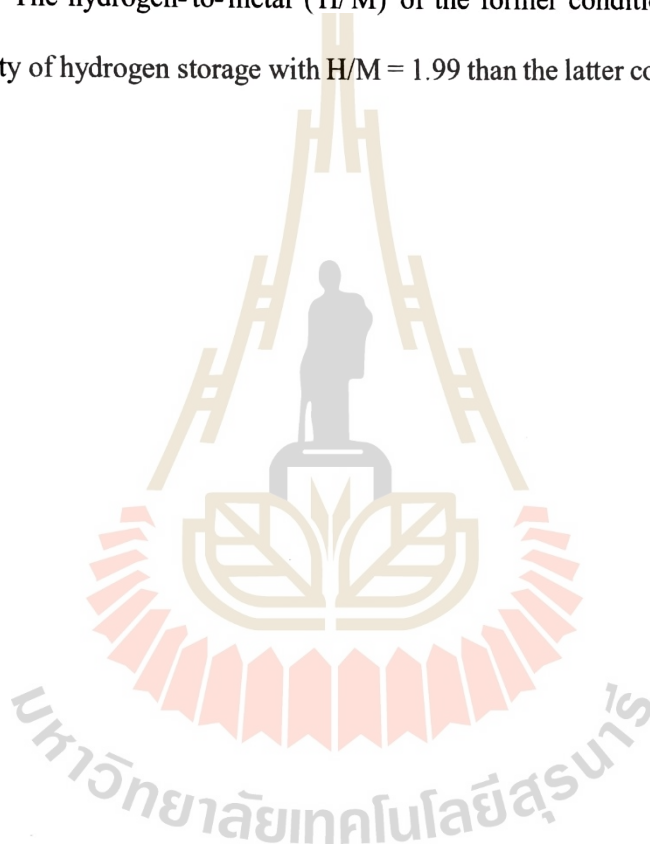
QUASICRYSTAL/MECHANICAL ALLOYING/HYDROGEN STORAGE/  
MAGNESIUM

This thesis aimed to study the improved capacity of hydrogen storage. Hydrogen is an interesting choice as alternative energy due to promising properties: clean, environmentally friendly, as well as being one of the most exuberant elements on earth. However, it is a truly challenging task to store hydrogen, since it must take safety concerns, cost conditions, the storage capacity, and the efficiency of the storage into account. Currently, many researchers have invented and come up with various techniques and methods of hydrogen storage. One of these interesting methods is the utilization of materials for hydrogen storage.

Ti-based quasicrystal alloy (Ti-Zr-Ni) was reported as an excellent hydrogen storage material with 140 sites of interstices, which are higher than the number of sites found in other crystals. Likewise, magnesium (Mg), is known as one of the most famous hydrogen reservoir materials due to the lower cost involved in its acquisition and good stability when reacting with hydrogen. However, the enthalpy and the temperature of  $\text{MgH}_2$  can become quite high during its hydrogen absorption, and the already available studies and research on Ti-Zr-Ni-Mg alloys are somewhat limited.

This research has been conducted by adding Mg into the Ti-Zr-Ni quasicrystal alloy as  $\text{Ti}_{45-x}\text{Zr}_{38}\text{Ni}_{17}\text{Mg}_x$ ;  $x=2, 4$ . The samples were mixed by mechanical alloying

under two conditions (1) 600 rpm with 20 h milling time and (2) 630 rpm with 30 h milling time. The samples were annealed to form quasicrystal. The gas-phase hydrogen absorption was observed by pressure composition isotherm (PCT) measurements. Morphology and structural analysis were, then, analyzed by XRD and SEM. The measurements showed the maximum capacity could be achieved by 600 rpm with 20 h milling time. The hydrogen-to-metal (H/M) of the former condition has revealed a higher capacity of hydrogen storage with  $H/M = 1.99$  than the latter condition with  $H/M = 1.58$ .



School of Manufacturing Engineering

Academic Year 2019

Student's Signature \_\_\_\_\_ นิตยา

Advisor's Signature \_\_\_\_\_ ๕

## **ACKNOWLEDGEMENTS**

This research could have not seen the light of day without support from numerous parties involving in the making. I am immensely grateful to all those, even from behind the curtain, whose involvement extended to such a great measure that I could not believe the completion of this study would be possible without them. Both financial support and facilities provided by the Suranaree University of Technology (SUT) and Shibaura Institute of Technology (SIT) in Japan were also deeply appreciated. My thanks go to Dr. Somsak Siwadamrongpong and Dr. Jittima Varagul, the thesis advisors who devoted their precious time and energy to give me valuable suggestions. Sincerely, I would like to thank Prof. Dr. Akito Takasaki, Prof. Dr. Susumu Uematsu, and Asst. Prof. Dr. Alicja klimkowicz for supporting and providing consistent supervision throughout my time in SIT, Japan. In addition, I would like to thank Amal Azraai Azuha and Keisuke Onoda. I greatly appreciate their generous help.

Finally, I would also like to express my deep sense of gratitude to the school of manufacturing engineering, which enables me to gain valuable opportunities and experiences throughout the course of this study at the Suranaree University of Technology.

Nitirut Phongsirimethi

# TABLE OF CONTENTS

	<b>Page</b>
ABSTRACT (THAI) .....	I
ABSTRACT (ENGLISH).....	II
ACKNOWLEDGEMENTS.....	IV
TABLE OF CONTENTS.....	V
LIST OF TABLES.....	VII
LIST OF FIGURES .....	VIII
<b>CHAPTER</b>	
<b>I INTRODUCTION</b> .....	1
1.1 General introduction.....	1
1.2 Research objectives .....	5
1.3 Scope and limitation of the study.....	6
<b>II LITERATURE REVIEW</b> .....	7
2.1 Material for Hydrogen storage .....	7
2.1.1 Magnesium (Mg) .....	7
2.1.2 Quasicrystals.....	11
2.1.3 Hydrogen storage in Ti-based quasicrystal powders.....	15
2.2 Literature review .....	17

## TABLE OF CONTENTS (Continued)

	<b>Page</b>
<b>III MATERIALS AND METHODS</b> .....	27
3.1 Materials.....	27
3.1.1 Parameters for calculation .....	27
3.1.2 Total atomic weight of $\text{Ti}_{43}\text{Zr}_{38}\text{Ni}_{17}\text{Mg}_2$ .....	28
3.1.3 Total sample weight of $\text{Ti}_{43}\text{Zr}_{38}\text{Ni}_{17}\text{Mg}_2$ .....	28
3.1.4 Amount weight of each powder of $\text{Ti}_{43}\text{Zr}_{38}\text{Ni}_{17}\text{Mg}_2$ .....	29
3.2 Sample preparations .....	29
3.3 The hydrogen absorption and desorption .....	30
<b>IV RESULTS AND DISCUSSION</b> .....	32
4.1 Analysis to identify appeared i-phase of $\text{Ti}_{45-x}\text{Zr}_{38}\text{Ni}_{17}\text{Mg}_x$ (x=2, 4) Compound.....	32
4.2 Analysis of the ability of hydrogen storage .....	41
4.3 Crystals phase.....	48
<b>V CONCLUSIONS</b> .....	49
<b>REFERENCES</b> .....	50
<b>BIOGRAPHY</b> .....	55

## LIST OF TABLES

Table	Page
2.1	Showed an overview of the scaffold to contain the $MgH_2/Mg$ ..... 10
2.2	Shown quasicrystalline class of each material ..... 15
2.3	Maximum hydrogen concentrations (H/M) in each material ..... 18
3.1	Calculate of the total atomic weight of $Ti_{43}Zr_{38}Ni_{17}Mg_2$ ..... 28
3.2	Calculate of the total sample weight (g) of $Ti_{43}Zr_{38}Ni_{17}Mg_2$ ..... 28
3.3	Calculate of the weight of each element of the $Ti_{43}Zr_{38}Ni_{17}Mg_2$ compound ..... 29
3.4	Materials Composition and Parameters ..... 30
4.1	The annealing temperature obtained from Differential scanning calorimetry (DSC) analysis of $Ti_{45-x}Zr_{38}Ni_{17}Mg_x$ , ( $x=2, 4$ ) compounds ..... 36
4.2	Estimated the hydrogen to metal atom (H/M) ratio with that of the other Ti-based i-phases ..... 48

## LIST OF FIGURES

Figure	Page
1.1 Show the hydrogen storage materials principle.....	3
1.2 Show and overview of the properties of the type of hydrogen storage materials .....	5
2.1 Illustration for the energy barrier and/or changing the reaction enthalpy of $MgH_2/Mg$ .....	8
2.2 Hydrogen absorption curves of $MgH_2$ fiber and $MgH_2$ powder.....	9
2.3 Show rotational symmetries of crystals 3-fold, 4-fold, and 6-fold axes .....	12
2.4 Show electron diffraction to possess icosahedral symmetry in combination.....	13
2.5 Simulations of some diffraction patterns.....	14
2.6 Simulations from an icosahedral quasicrystal .....	14
2.7 Shown Bergman two-shell cluster of $Ti_{36}Zr_{32}Ni_{13}$ .....	16
2.8 Shown crystal structure (a) face-centered cubic type (b) body-centered cubic type .....	17
2.9 Schematic diagram of a ball mill.....	20
2.10 Planetary ball mill machine (Fritsch Pulverisette-7).....	21
2.11 Single-roller melt-spinning apparatus .....	22
2.12 Shown conditions for diffraction and derivation of Bragg's law.....	23
2.13 Shown wave interference of constructively and destructively .....	24

## LIST OF FIGURES (Continued)

Figure	Page
2.14 Shown (a) X-ray scattering patterns of the amorphous phase, (b) X-ray scattering patterns of crystal and quasicrystals phase ( $\text{Ti}_{45}\text{Zr}_{38}\text{Ni}_{17}$ ) were observed peaks.....	25
2.15 Schematic of the PCT Sieverts' apparatus. PT, PCT pressure gauge; EDV, PCT measuring section empty cell; SC, Sample cell; MMV-1 and MMV-2, Flow regulating valves; $\text{H}_2$ , Hydrogen valve <sup>a</sup> ; Sample, Sample valve <sup>a</sup> , Vac <sup>a</sup> and Vac (Rough) <sup>a</sup> .....	27
4.1 The X-ray diffraction patterns for $\text{Ti}_{45-x}\text{Zr}_{38}\text{Ni}_{17}\text{Mg}_x$ , ( $x=2, 4$ ) compounds after the mechanical alloying process .....	33
4.2 Differential scanning calorimetry of $\text{Ti}_{45-x}\text{Zr}_{38}\text{Ni}_{17}\text{Mg}_x$ , ( $x=2, 4$ ) compounds after the mechanical alloying process .....	35
4.3 The X-ray diffraction patterns $\text{Ti}_{45-x}\text{Zr}_{38}\text{Ni}_{17}\text{Mg}_x$ , ( $x=2, 4$ ) compounds after annealing .....	38
4.4 Particles of size by SEM measurements.....	40
4.5 Hydrogen absorption and desorption pressure-composition .....	42
4.6 X-ray diffraction patterns for the i-phase powder, Rotation speed 600 rpm, 20 h.....	44
4.7 Result of SEM analysis to compare the surface morphology of compounds before and after the hydrogenation process. ....	46

# CHAPTER I

## INTRODUCTION

### 1.1 General introduction

It is an undeniable fact that fossil fuels are the primary fuel source used in the present time and various sectors such as transportation, industrials, agriculture, and so forth. However, fossil fuels are depleting rapidly due to the growingly excessive need for energy. A steady increase in population is one of the main reasons that leads to the increasingly energy-consuming demand and significantly higher emissions of greenhouse gases caused by the burning of fossil fuel. As a result, many researchers have studied and researched sustainable energy sources that can be used as alternative energy in the future. (Durbin et al. 2013)

Hydrogen has the potential to be utilized as an alternative energy source in the present due to the highest heating value per mass when compared to other chemical fuels, its environmental friendliness, and its natural availability. It was reported that hydrogen has the highest energy density compared to other fuels by weight. However, not without any disadvantages, hydrogen gas also has the lowest energy density by volume, and more importantly, hydrogen gas could explode violently when exposed to air. Therefore, it is a truly challenging task for researchers to store hydrogen since they must take safety concerns, cost conditions, storage capacity, and the efficiency of the storage into account.

Currently, there are various methods of hydrogen storage such as (1) storage in its gaseous form, (2) liquefaction, (3) cryo-compression, and (4) material storage.

Although the first option is commercially available, there persist some technical flaws e. g. low volumetric capacity and high compression energy. The second alternative, liquefaction, can produce high energy. Nevertheless, it is expensive and has safety issues, due to the constant concern overheat control to reduce the chance of boiling off. The cryo-compression option can get a high volumetric capacity but it requires high energy to be used for liquefaction. For the last option, material storage, its primary disadvantages are low gravimetric/volumetric capacity and high operating temperature for H<sub>2</sub> release. However, the utilization of materials to store hydrogen is much safer than any other method provided above. That is because if the hydrogen-carrying tank is damaged, then the stored hydrogen gas will not promptly be released. The hydrogen gas is still absorbed in the material unless the temperature gets to a certain degree that ensures bond dissociation as shown in figure 1.1. Despite the imperfections, hydrogen storage materials still have continuously been researched, studied, and improved.

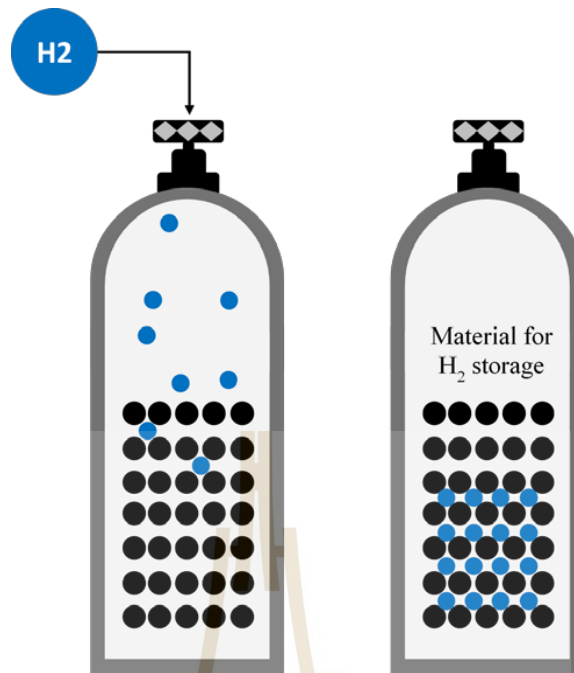


**Figure 1.1** Show the hydrogen storage materials principle

The hydrogen storage materials have four major types as follows:

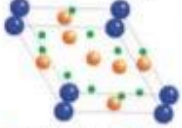
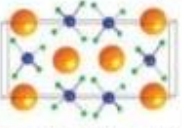
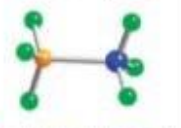
(1) Chemical hydrides; this type of hydrogen storage uses the principle of chemically bound hydrogen with materials. They could contain large quantities of hydrogen by mass and volume. However, chemical hydrides are not rechargeable. Therefore, they are mostly used in single-use applications such as in rockets to send probes to outer space.

(2) Complex hydrides; they have large gravimetric/ volumetric capacity but not as large as those of chemical hydrides. Complex hydrides can reverse hydrogen kept in the storage, therefore, they have attracted great interest in the field of hydrogen storage. Materials complex hydrides consist of, for instance, lithium ( $\text{LiAlH}_4$ ), lithium amide ( $\text{LiNH}_2$ ), magnesium hydride ( $\text{MgH}_2$ ), and quasicrystal (Ti-Zr-Ni) etc.

Magnesium (Mg) is one of many interesting choices to be used as hydrogen storage due to its high hydrogen capacity of up to 7.6 wt.% (Zaluski et al., 1995). If Mg forms chemical bonding with other elements such as Nickel (Ni), it will be transformed into  $Mg_2Ni$  which can be used to store hydrogen efficiently

Quasicrystal was also shown to have the potential to be hydrogen storage because it has a higher number of interstices than those found in other crystals. (Takasaki and Kelton, 2006).

(3) Sorbents; this method of using sorbents is a way to utilize their porous qualification to store hydrogen. The sorbent materials are lightweight and have high surface areas. Besides, they can reverse and kinetically discharge (charge) hydrogen very well. However, this method causes chemically weak bonding between molecular hydrogen and the sorbent at the operating temperature of 196 °C. Therefore, the studies of sorbent materials aim to strategically increase the strength of hydrogen bonding. Figure 1.2 shows an overview of the properties of the type of hydrogen storage materials (Yang et al. 2009).

	Conventional Hydrides	Complex Hydrides	Sorbent Systems	Chemical Hydrides
	Ex. $\text{LaNiH}_6$  ● = H ● = La ● = Ni Hydrogen forms a metallic bond with the host metal atoms	Ex. $\text{NaAlH}_4$  ● = H ● = Al ● = Na Hydrogen covalently bonded as stable "complex" anions	Ex. MOF-5  ● = $\text{H}_2$ accessible surface Physisorption of molecular hydrogen to high surface area sorbent	Ex. $\text{NH}_3\text{BH}_3$  ● = H ● = N ● = B Hydrogen covalently bonded in material & utilized as single use 'fuel'
<b>General Trends</b>				
Vol. Capacity	G	G	Y	G
Grav. Capacity	R	G	G	G
Reversibility	G	G	G	R
Thermodynamics	G	G	R	Y
Kinetics	G	R	G	Y
Efficiency	G	G	G	R

**Figure 1.2** shows an overview of the properties of the type of hydrogen storage materials.

This research aims to study the potential of hydrogen storage. My main interest lies in the hydrogen storage built from complex hydrides materials. Furthermore, I study the appearance of quasicrystal in Ti-Zr-Ni-Mg compound materials, which is a mixture of two materials, namely quasicrystal, and Mg.

## 1.2 Research objectives

1.2.1 To study the appearance of quasicrystal in the Ti-based composition of  $\text{Ti}_{43}\text{Zr}_{38}\text{Ni}_{17}\text{Mg}_2$  compound.

1.2.2 To study the hydrogen absorption capacity (hydrogen-to-metal ratio) of hydrogen storage of the  $\text{Ti}_{43}\text{Zr}_{38}\text{Ni}_{17}\text{Mg}_2$  compound.

### 1.3 Scope and limitation of the study

1.3.1 The study concerns specifically the quasicrystal type of Ti-base (Ti-Zr-Ni).

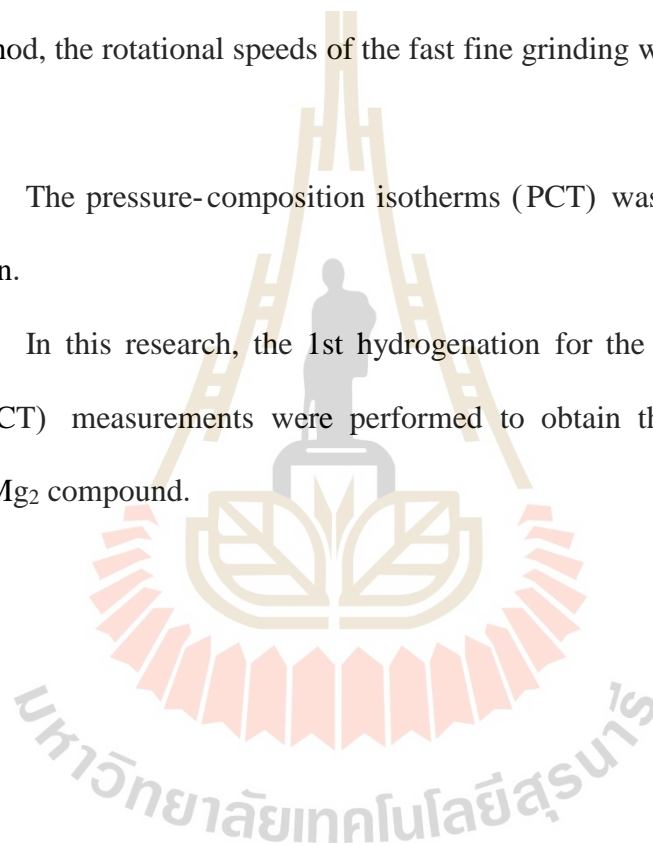
1.3.2 The ball to powder ratio was 8:1.

1.3.3 The sample for hydrogen storage was powder.

1.3.4 To study mixing samples of hydrogen storage with the mechanical alloying method, the rotational speeds of the fast fine grinding were set at a maximum of 800 rpm.

1.3.5 The pressure-composition isotherms (PCT) was used as a method of hydrogenation.

1.3.6 In this research, the 1st hydrogenation for the pressure composition isotherm (PCT) measurements were performed to obtain the H/ M ratio of the  $\text{Ti}_{43}\text{Zr}_{38}\text{Ni}_{17}\text{Mg}_2$  compound.



# CHAPTER II

## LITERATURE REVIEW

### 2.1 Material for Hydrogen storage

In the present time, researchers have invented the technology, apparatuses, and many methods for hydrogen storage. One of the methods is hydrogen storage constructed from complex hydrides materials. The principle of this method is to use materials and making it chemical bonding with or absorbing hydrogen, instead of having hydrogen being stored directly in the tank. The primary materials used as a storage of hydrogen gas are as follows.

#### 2.1.1 Magnesium (Mg)

Magnesium hydride has a high potential of hydrogen capacity and has high thermodynamic stability to store hydrogen of 7.6 wt% (Wang and Wang, 2017; Jain et al., 2010). However, the enthalpy and temperature for hydrogen absorption can get very high which leads to high operation temperature ( $> 350\text{ }^{\circ}\text{C}$ ).

In addition,  $\text{MgH}_2$  could be slow sorption kinetics if an oxide appeared on the surface of  $\text{MgH}_2$  (Figure 2.1). However, Wang and Wang, 2017 reported that there were many methods for improving hydrogen sorption properties of magnesium hydride such as alloying, nanoscaling, nanoconfinement, adding catalysts, and mixing with other metal hydrides.

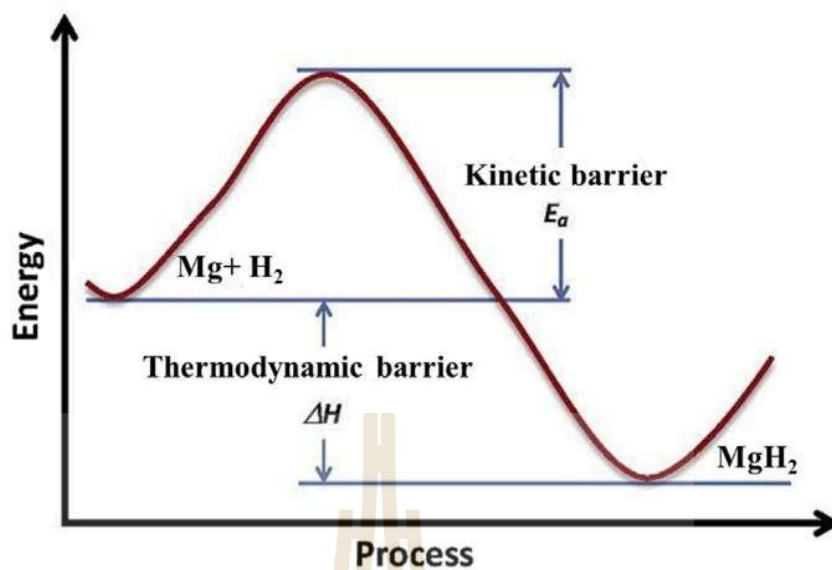


**Figure 2.1** Illustration for the energy barrier and/or changing the reaction enthalpy of MgH<sub>2</sub>/Mg Wang and Wang, 2017

#### 2.1.1.1 Alloying

Alloying is a method aimed to reduce the thermodynamic of magnesium hydride. The principle of the alloying method is that by adding other elements or compounds into Mg-based, it can result in reducing stability and the decreasing operation temperature of MgH<sub>2</sub>/Mg. Various elements and compounds, such as Nickel (Ni), have been used to combine with Mg. The possible result of the combination between Ni with Mg is Mg<sub>2</sub>Ni or Mg<sub>2</sub>NiH<sub>4</sub> in the hydride form, which has a hydrogen storage capacity of H/M = 1.33 (Ueda et al., 2005).

#### 2.1.1.2 Nanoscaling

The principle of nanoscaling is that by reducing the grain size of MgH<sub>2</sub> to less than 3 nm, it can result in the improvement of thermodynamic and kinetics due to the increased surface of the compound and the decreased diffusion

distance of hydrogen. However, some drawbacks occurring in the cycling of nanoscaling persist due to the aggregation of particles during cycling. Figure 2.2 shows the isothermal absorption curves of this  $\text{MgH}_2$  fiber and  $\text{MgH}_2$  powder. It shows that hydrogen storage of  $\text{MgH}_2$  fiber has a higher potential than  $\text{MgH}_2$  powder. Besides, a mere minor change in the size of the particles may differently result in the absorption of hydrogen. Therefore, in the preparation of nanoscaling, a certain appropriate size must first be determined. (Wang and Wang., 2017).

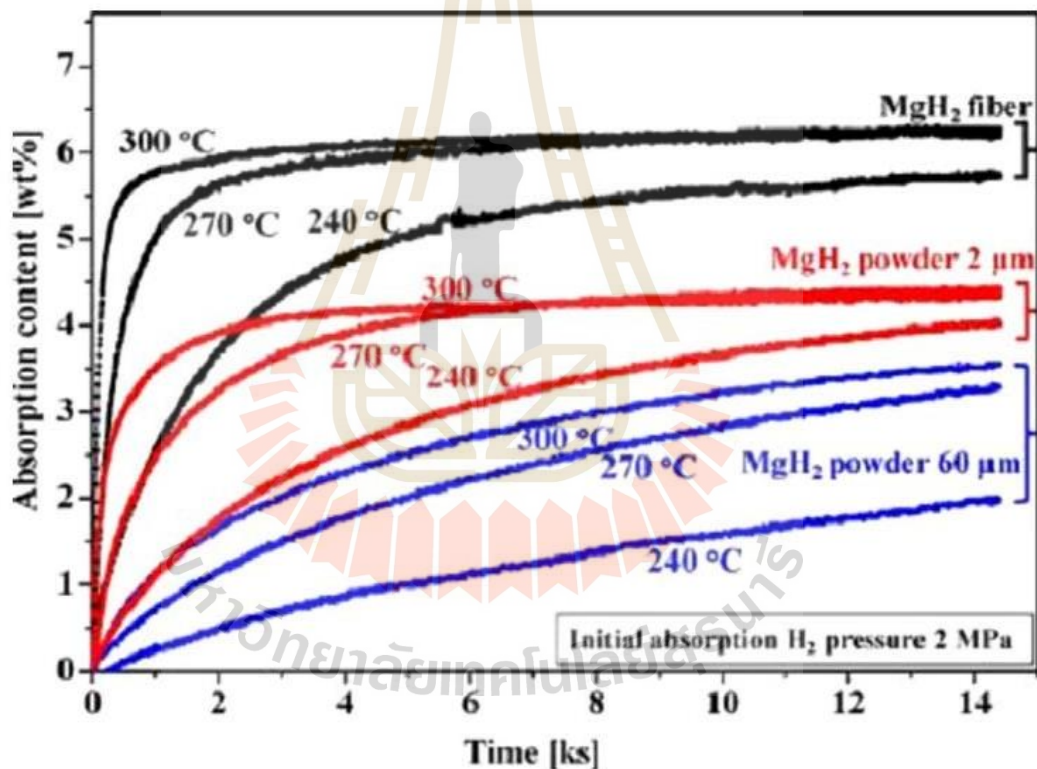


**Figure 2.2** Hydrogen absorption curves of  $\text{MgH}_2$  fiber and  $\text{MgH}_2$  powder

### 2.1.1.3 Nanoconfinement

In order to reduce the problem of nanoscaling about the aggregation of particles during cycling, the nanoconfinement method was invented to

solve the problem stated above by embedding the  $Mg_2H/Mg$  through the nanoscaling method into a stable scaffold. Table 2.1 shows an overview of the scaffold to contain the  $Mg_2H/Mg$  (Wang and Wang., 2017). Requirements for the scaffold materials are as follows: (1) chemical inertness (2) high volume ratio and uniform pore size distributions (3) high surface area (4) structural stability. However, the cycle stability of  $Mg_2H$  is not that stable because its capacity after going through the nanoconfinement method decreases due to the limited loading amount.

**Table 2.1** Showed an overview of the scaffold to contain the  $MgH_2/Mg$  (Wang and Wang., 2017)

Sample	Pore size (nm)	Precursor	Solvent/ Atmosphere	Loading (%wt)
RF-CA <sup>a</sup> / $MgH_2$	22	$MgBu_2$	Heptane/Ar	18.2
RF-CA / $MgH_2$	7	$MgBu_2$	Heptane/Ar	10.0
RF-CA / $MgH_2$	13	$MgBu_2$	Ar	14.8
AC(fiber) <sup>b</sup> / $MgH_2$	0.5-3	$MgBu_2$	Ar	22.0
RF-CA(Ni) / $MgH_2$	13	$MgH_2$	Ar	9.6
RF-CA(Cu) / $MgH_2$	13	$MgH_2$	Ar	12.7
RF-CA / $MgH_2$	13	$MgH_2$	Ar	3.6
HSAG <sup>c</sup> / $MgH_2$	2-3	$MgH_2$	Ar	10-15
AC <sup>d</sup> / $MgH_2$	<2	$MgH_2$	Ar	15-20
CA / $MgH_2$	6-20	$MgH_2$	Ar	10
CMK-3 / $MgH_2$	3.9	$MgBu_2$	Heptane/Ar	20

<sup>a</sup> Resorcinol–formaldehyde carbon aerogels.

<sup>b</sup> Carbon aerogels.

<sup>c</sup> High surface area graphite.

<sup>d</sup> Activated carbon.

#### 2.1.1.4 Adding catalysts

It is important that the energy barrier and/or the changing reaction enthalpy of  $\text{MgH}_2/\text{Mg}$  must be improved. Adding catalysts into  $\text{MgH}_2/\text{Mg}$  is the easiest method to increase the effectiveness of hydrogen storage. The principle of catalysts is that by adding substance or compounds into the initiative material, it can decrease or change the reaction enthalpy, and can increase the kinetics of the chemical reaction.

The catalysts that were used in the experiment are as follows: The  $\text{Mg}_2\text{H}$  with G-Fe in the system released hydrogen temperature at 281 °C and showed a lower energy barrier of 119  $\text{kJ mol}^{-1}$  etc. (Wang and Wang., 2017).

#### 2.1.1.5 Mixing with other metal hydrides

Combining  $\text{MgH}_2$  with other metal hydrides leads to a new chemical bonding which could also improve the thermodynamic and kinetic of  $\text{Mg}_2\text{H}$ . For example, if aluminum hydrides ( $\text{AlH}_3$ ) was mixed with  $\text{MgH}_2$ , then the dehydrogenation process of this new system would be complex hydride  $\text{Al}_{12}\text{Mg}_{17}$  phases (Jain et al., 2010).

### 2.1.2 Quasicrystals

#### 2.1.2.1 Crystals

Common crystals have an orderly and a three-dimensional periodic arrangement of atoms and molecules. The crystal structure has a pattern that regularly repeats of unit-cells and infinitely extends until space is filled up. This characteristic is called translational symmetry.

One of the most important characteristics of crystals is rotational symmetry. It was reported that crystals can only have the rotational symmetries of 2-fold, 3-fold, 4-fold, and 6-fold axes (Figure 2.3). Thus, when considering figure 2, only the axes of 3-fold, 4-fold, or 6-fold have rotational symmetry, therefore they are considered crystals. While, the 5-fold, 8-fold, 10-fold, or 12-fold symmetry axes are not.

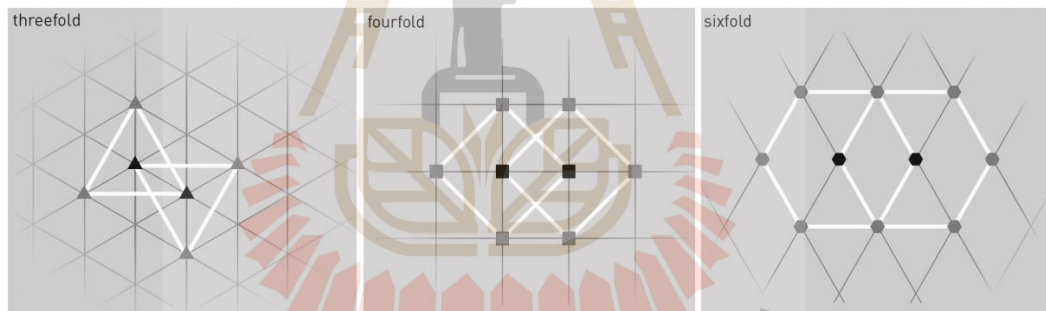


**Figure 2.3** Show rotational symmetries of crystals 3-fold, 4-fold, and 6-fold axes

#### 2.1.2.2 Quasicrystals

Quasicrystals were discovered by Shecht man et al. (1984). They are materials with long-range order like normal crystals. However, they are not three-dimensional translational order like 5-fold, 8-fold, 10-fold, or 12-fold symmetry axes which are disallowed in normal crystals. The first group of quasicrystals is aluminum (Al) with a 10-14% manganese (Mn) alloy. This kind of quasicrystal

(aluminum (Al) with 10-14% manganese (Mn) alloy) shows electron diffraction to possess icosahedral symmetry in combination (Figure 2.4).

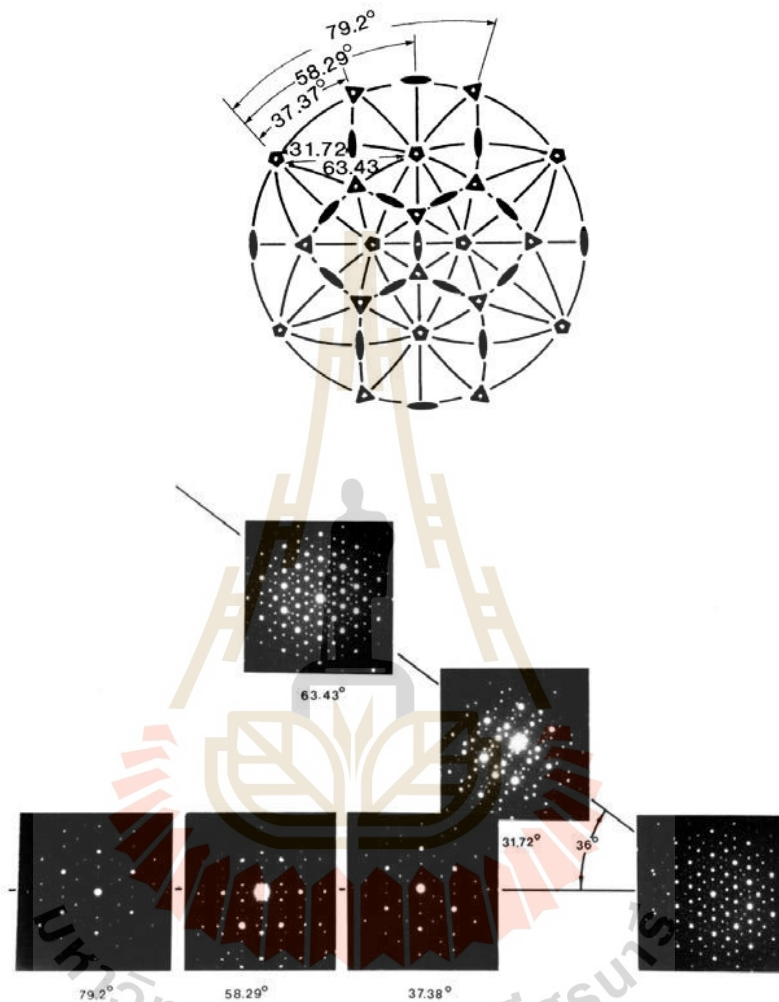


**Figure 2.4** Shows electron diffraction to possess icosahedral symmetry in combination (Shechtman et al., 1984).

There are two type of quasicrystals, which include (1) polygonal quasicrystals or dihedral quasicrystal group and (2) icosahedral quasicrystals. The polygonal quasicrystals could be said that this group of quasicrystals are periodic in one axis or axial symmetry Octagonal quasicrystal (8- fold symmetry), Decagonal

quasicrystal (10-fold symmetry), Dodecagonal quasicrystal (12-fold symmetry) shown in Figure 2.5

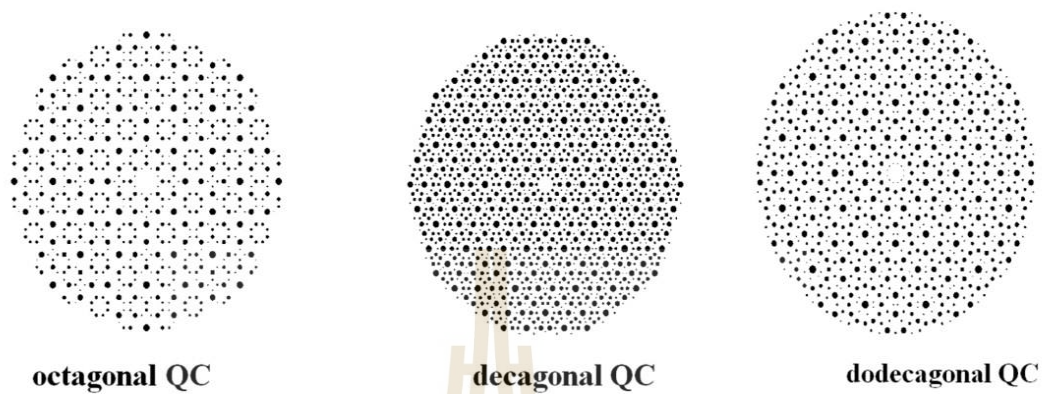


**Figure 2.5** Simulations of some diffraction patterns (Samavat,, 2012).

Another group of quasicrystals is the icosahedral quasicrystals. This group of crystal has no periodic direction, as shown in Figure 2.6.

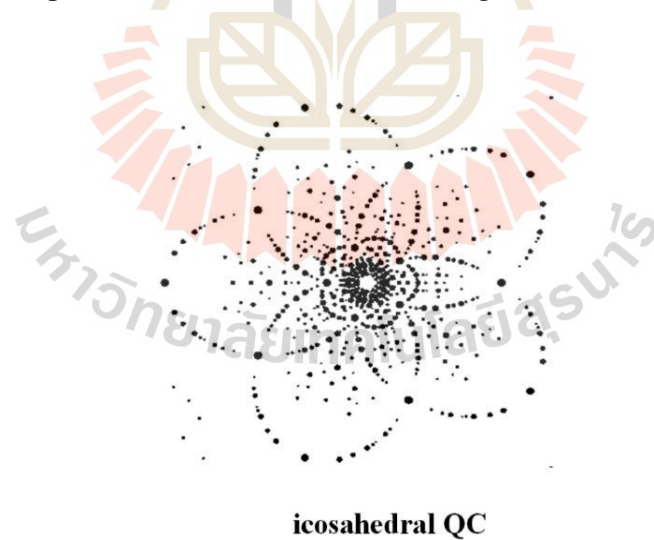


**Figure 2.6** Simulations from an icosahedral quasicrystal (Samavat,, 2012)

The data has been collected from various materials with the structure of quasicrystal. The quasicrystalline class can be summarized as in Table 2.2

**Table 2.2** Shown quasicrystalline class of each material (Samavat,., 2012).

<b>Octagonal quasicrystal</b>	<b>Decagonal quasicrystal</b>	<b>Dodecagonal quasicrystal</b>	<b>Icosahedral quasicrystal</b>
V-Ni-Si	Al-Cu-Mn	Cr-V-Ni	Al-Mn
Mn-Si	Al-Cu-Fe	V-Ni	Al-Mn-Si
Mn-Si-Al	Al-Cu-Ni	V-Ni-Si	Al-Li-Cu
Mn-Fe-Si	Al-Cu-Co		Al-Pd-Mn
	Al-Cu-Co-Si		Al-Cu-Fe
	Al-Mn-Pd		Al-Mg-Zn
	V-Ni-Si		V-Ni-Si
	Cr-Ni		Pd-U-Si
			Ti-Ni-based

### 2.1.3 Hydrogen storage in Ti-based quasicrystal powders

One of the most famous compounds is Ti-based quasicrystal (Ti-Zr-Ni). A ti-based quasicrystal is the second largest group of the stable quasicrystals, which was the thermodynamically stable, strong in chemical affinity with hydrogen, and inexpensive. Especially, the icosahedral phase (i-phase) in quasicrystal showed a very high hydrogen storage capacity. The height in the capacity is because they contain more tetrahedral interstitial sites than normal crystal and have the structure of the Bergman two-shell atomic cluster. The reports indicated that Bergman two-shell cluster contained 20 tetrahedral interstitials within its inner shell and 120 between its inner and outer shells show in Figure 2.7 (Takasaki and Kelton, 2006).

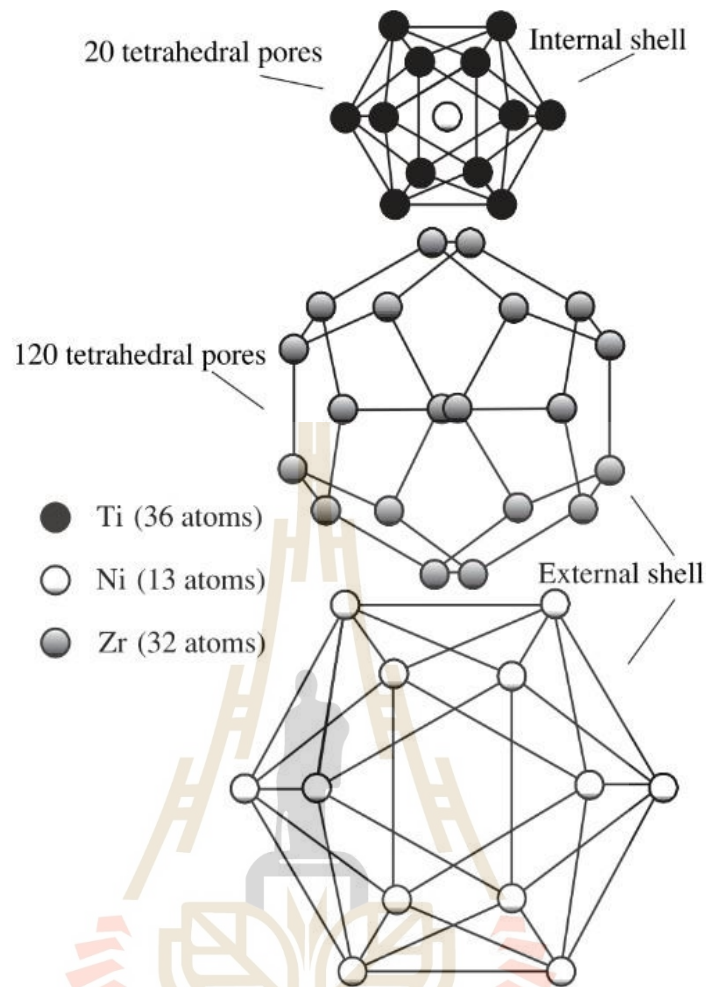


**Figure 2.7** Shows Bergman two-shell cluster of  $\text{Ti}_{36}\text{Zr}_{32}\text{Ni}_{13}$  (Morozov et al., 2006).

It was reported that the total number of interstices per one normal crystal lattice observed as the crystal structure of face-centered cubic (fcc) type had 13 octahedral sites and 8 tetrahedral sites and body-centered cubic (bcc) type had 18 octahedral sites and 24 tetrahedral shown in Figure 2.8. It is clear that the total number of i-phase is higher than the number of interstices in normal crystal. Therefore, it can be concluded that it is suitable sites for hydrogen storage (Takasaki and Kelton, 2006).

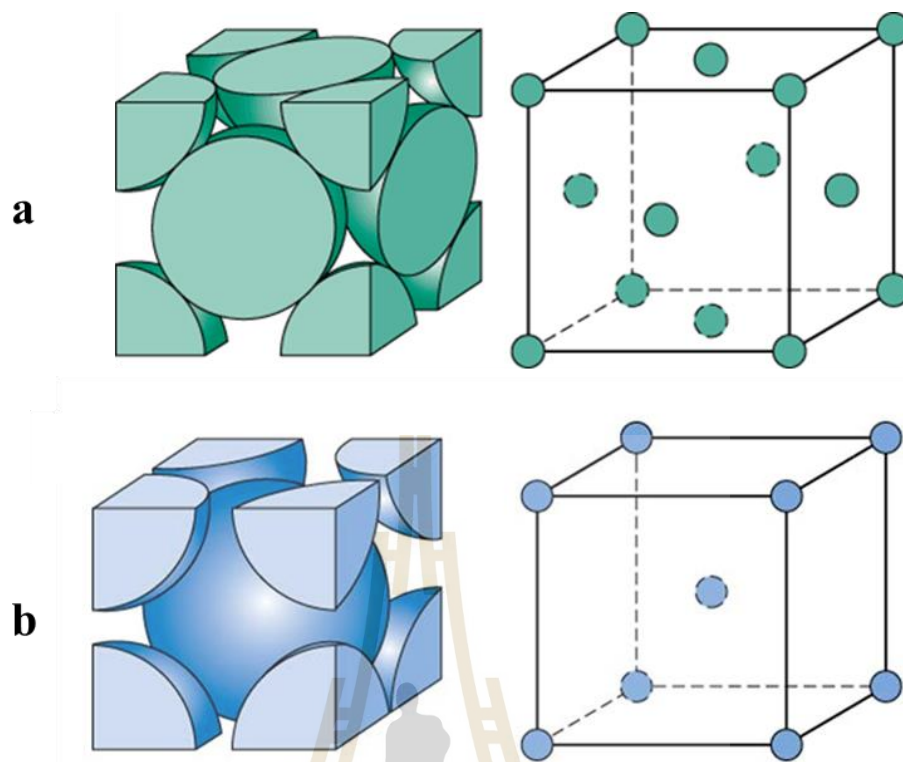


**Figure 2.8** Shown crystal structure (a) face-centered cubic type (b) body-centered cubic type.

## 2.2 Literature review

To improve the ability of hydrogen storage, many researchers have attempted to search for various materials, methods, and technology that will enable them to do so.

### 2.2.1 Hydrogen-storing Capability of Materials

Up to this point in time, there are many types of materials for hydrogen storage as mentioned. Each material has different characteristics and hydrogen storage capacities. To specify hydrogen storage capacity, there are many methods to explain but the generally accepted method is the hydrogen to metal (H/M).

The hydrogen to metal (H/M) ratio could be obtained by the following equation; proposed by Viano et al. (2010).

$$\frac{H}{M} = \frac{a_q^H - a_q^0}{0.1974} \quad (1)$$

From the equation,  $a_q^H$  represents quasi-lattice parameter at the hydrogen concentration of interest and  $a_q^0$  measured quasi-lattice parameter for the non-hydrogenated i-phase. The value 0.197 was measured from a slope of the quasi-lattice that expands linearly with hydrogen concentration.

From studies and various researches on materials for hydrogen storage, the results of the hydrogen to metal (H/M) ratio are summarized in table 2.3.

**Table 2.3** Maximum hydrogen concentrations (H/M) in each material.

Authors	Sample	Sample preparation	Hydrogenation method	(H/M) ratio
Azuha et al., 2020	Ti <sub>45</sub> Zr <sub>38</sub> Ni <sub>12</sub> Cr <sub>5</sub> (powder)	ball-milling	Electrochemical	1.36
Azuha et al., 2020	Ti <sub>45</sub> Zr <sub>38</sub> Ni <sub>7</sub> Cr <sub>10</sub> (powder)	ball-milling	Electrochemical	1.29
Azuha et al., 2020	Ti <sub>45</sub> Zr <sub>38</sub> Cr <sub>17</sub> (powder)	ball-milling	Electrochemical	1.22
Takasaki et al., (2006)	Ti <sub>41</sub> Zr <sub>42</sub> Ni <sub>17</sub> (powder)	ball-milling	Electrochemical	1.74

Authors	Sample	Sample preparation	Hydrogenation method	(H/M) ratio
Takasaki et al., (2006)	Ti <sub>40</sub> Hf <sub>40</sub> Ni <sub>20</sub> (powder)	ball-milling	Electrochemical	1.20
Nobuki et al., (2019)	Ti <sub>2</sub> Ni (powder)	ball-milling	Gaseous	0.83
Tomoki et al., (2019)	Ti <sub>45</sub> Zr <sub>38</sub> Ni <sub>17</sub> (powder)	ball-milling	Gaseous	1.30
Shahi et al., (2011)	Ti <sub>45</sub> Zr <sub>38</sub> Ni <sub>17</sub> (ribbons)	melt spinning	Gaseous	1.87
Jayalakshmi et al., (2006)	Ti <sub>50</sub> Zr <sub>25</sub> Cu <sub>25</sub> (ribbons)	melt spinning	Electrochemical	1.20
Ueda et al., 2005	MgNi <sub>2</sub> H <sub>4</sub> (powder)	ball-milling	Gaseous	1.33

### 2.2.2 Sample preparation

Ti-based is one of the quasicrystals used to store hydrogen gas. Various researchers have tried to increase its ability to store hydrogen by mixed other elements into the Ti-based, such as Ti<sub>45</sub>Zr<sub>38</sub>Ni<sub>17</sub>, Ti<sub>50</sub>Zr<sub>25</sub>Cu<sub>25</sub>, Ti<sub>60</sub>Zr<sub>15</sub>Ni<sub>15</sub>Cu<sub>10</sub>, or Ti<sub>45</sub>Zr<sub>38</sub>Ni<sub>12</sub>Cr<sub>5</sub>, etc. Even after adding various elements into Ti-based, it has still retained its quasicrystal structure. The mixing methods used to prepare quasicrystal are provided as follows.

### 2.2.2.1 Mechanical alloying (ball-milling)

Mechanical alloying (MA) is a metal powder processing technique to produce a homogeneous material using the high-energy ball to milling. Currently, mechanical alloying is an important method and is widely used and applied, including in the studies of hydrogen storage (Suryanarayana, 2019).

The principle of mechanical alloying is that by mixing the alloy materials powder and balls mill into the vials or chamber, the mill then rotates, and the balls mill ground the materials to a fine powder (Figure 2.9-2.10).

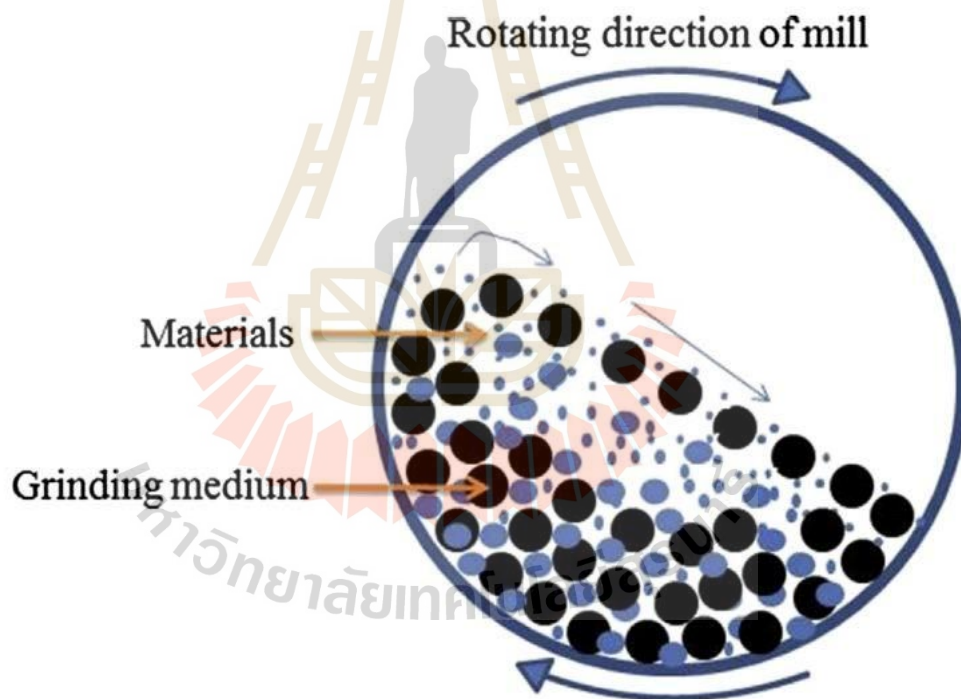


**Figure 2.9** Schematic diagrams of a ball mill (Khadka et al., 2014).



**Figure 2.10** Planetary ball mill machine (Fritsch Pulverisette-7)

Mechanical alloying (MA) uses balls to mill substances to powder. Therefore, the ratio of ball to powder and the space in the chamber has to be appropriate for milling. It is reported that the proportion of ball should be about 40-50 percent of space in the chamber and powder should be about 25 percent.

For the ratio of ball to powder, Hosni et al. (2017), reported the results of his studies on the structural and electrochemical properties of TiFe alloys synthesized by ball milling for hydrogen storage and ball to powder weight ratios (2:1, 5:1, and 8:1) to optimize the milling parameters. It is found that the ball to powder weight ratios of 8:1 was the optimized milling parameters. From the XRD results, it showed that the ball to powder weight ratios of 8:1 has the highest conversion rate to TiFe.

#### 2.2.2.2 Melt spinning

The melt-spinning is one of the sample preparation technologies for making hydrogen storage. This method is followed by the use of the

rapid cooling of molten liquids by roller. The rollers have two types, twin-roller, and single-roller. They were introduced to produce rapidly solidified metallic ribbons (Figure 2.11). Currently, the single-roller method is more favored than the twin-roller due to its simplicity and reproducibility (Rong et al., 2018). The melt-spinning method leads to an interesting physical characteristic of the sample, which is formed into the shape of ribbons. In this particular shape, the sample gains more microstructure, and surface area for storing hydrogen, leading to attractive hydrogen capacity and kinetics of hydrogen absorption (Leiva et al., 2012).

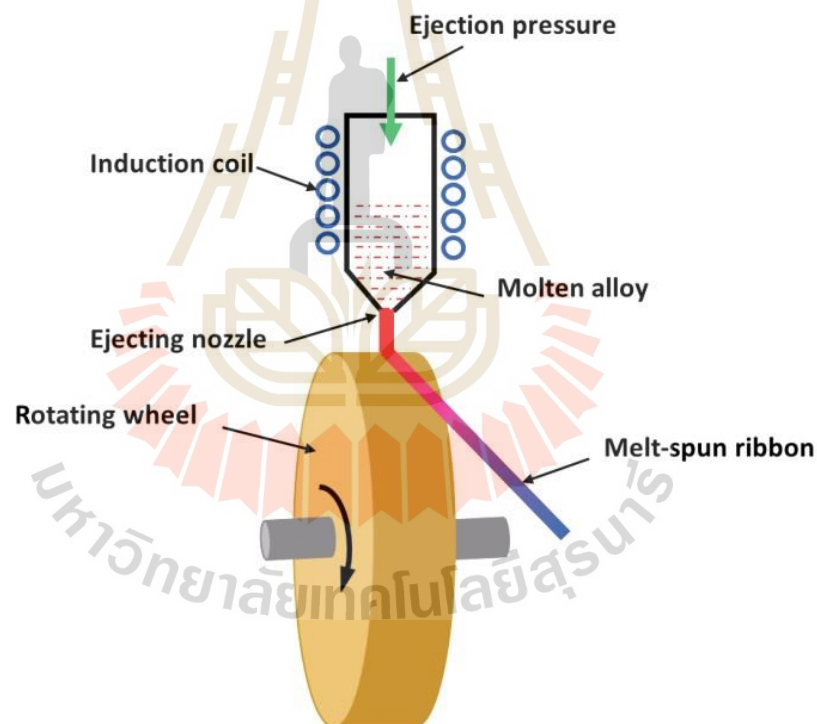


**Figure 2.11** Single-roller melt-spinning apparatus (Rong et al., 2018).

### 2.2.3 X-ray diffraction (XRD) measurements

Before the discovery of X-rays by Wilhelm Conrad Roentgen in 1895 (Epp, 2016), scientists had deduced that crystals had an orderly periodic arrangement

of atoms and molecules. After the discovery of X-rays, scientists were able to explain the characteristics more precisely and can see the details inside the crystals structure. X-ray diffraction (XRD) measurements is a method used to identify the element of minerals or compounds.

The principle of the methods is that the diffraction of X-rays beam occurs by having a different optical path length to travel. The magnitude of this path length depends on the distance of the layer of crystal and the incident angle of the X-ray beam (Figure 2.12). This is summarized in the Bragg's law Equation

$$n\lambda = 2d\sin\theta \quad (2)$$

Where  $n$  is a parameter of integer (order of diffraction),  $\lambda$  is the wavelength of the x-rays (nm),  $d$  is the spacing between planes in the atomic lattice of the sample, and  $\theta$  is the diffraction angle in degrees.

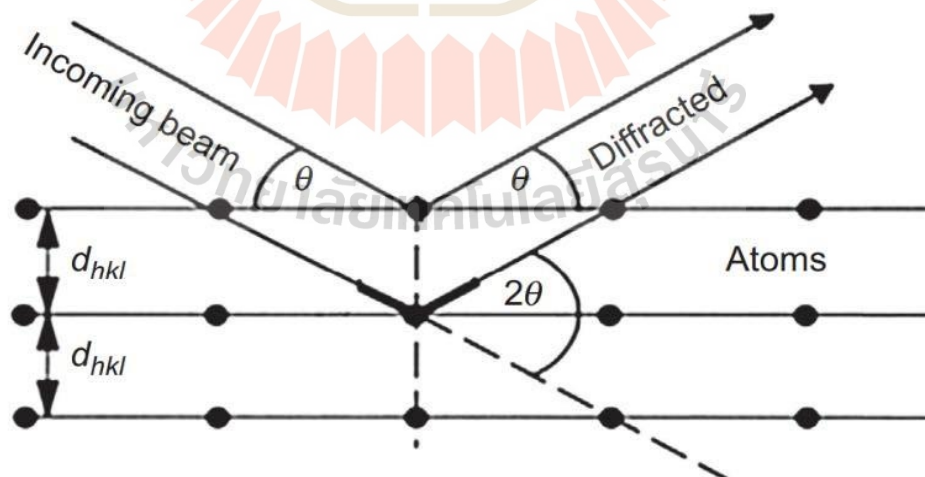


**Figure 2.12** Shown conditions for diffraction and derivation of Bragg's law

(Epp, 2016)

The X-ray beam is scattered at different planes of the material. The detectors of X-ray diffraction, then, read the signal waves. If they have the same alignment after that the signal is amplified, then the signal is constructive interference. However, if the signal waves are out of alignment, then that the signal is destructive interference. Both types of interferences are shown in Figure 2.13.

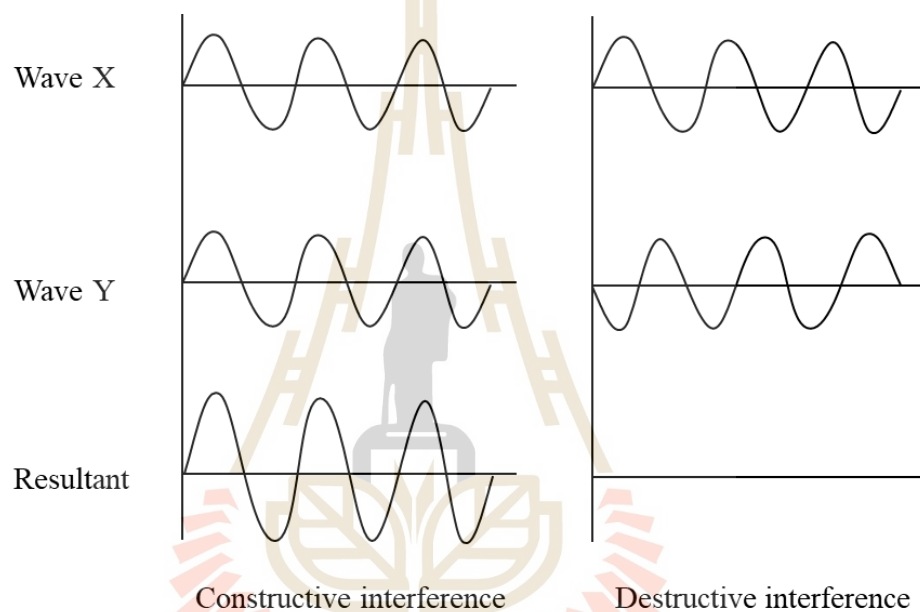


**Figure 2.13** Shows wave interference of constructively and destructively.

The X-ray diffraction (XRD) measurements are used to identify the characteristics of materials. The X-ray scattering patterns were dependent on each material. If the observed signal waves are amplified (constructive interference), peaks will appear in X-ray scattering patterns. That means the material could have a periodic arrangement of atoms and molecules (crystal phase). However, if the signal waves are destructive interference, that means it could be an amorphous phase as shown in Figure 2.14.

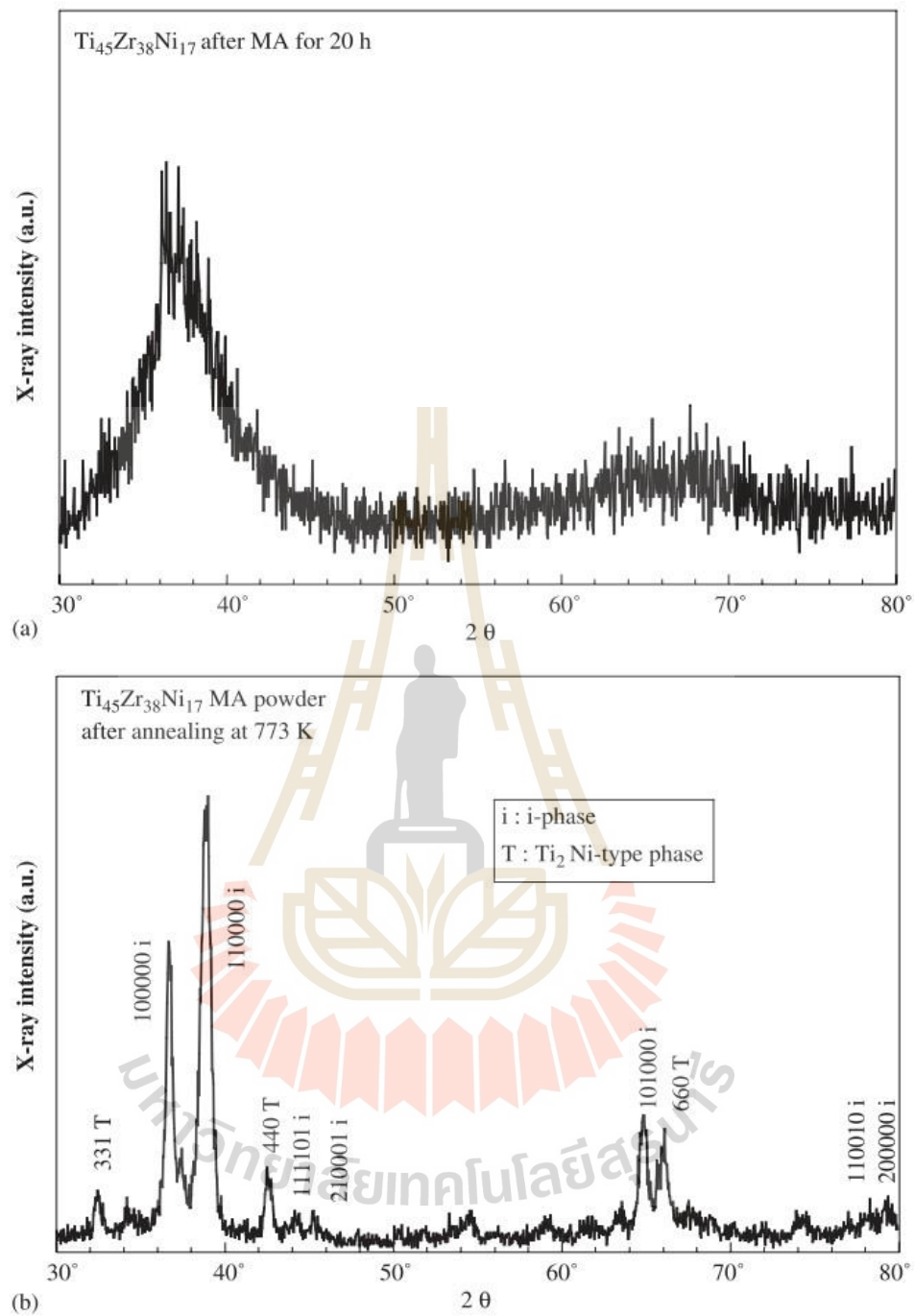


**Figure 2.14** Shows (a) X-ray scattering patterns of the amorphous phase, (b) X-ray scattering patterns of crystal and quasicrystals phase ( $\text{Ti}_{45}\text{Zr}_{38}\text{Ni}_{17}$ ) were observed peaks. (Takasaki and Kelton. 2006).

## 2.2.4 Hydrogenation

### 2.2.4.1 Gaseous

The technic of the hydrogenation method by feeding the hydrogen in the state of gaseous into the material. The determined hydrogen absorption and desorption, and the pressure-composition isotherms (PCT) were measured at a constant temperature by a Sieverts-type apparatus (Takasaki and Kelton, 2006). The principle of this method is that the hydrogen-free sample powder in the standard approximate weight of 0.5 g was poured into the vessel (SC) shown in Figure 2.15. Then the vessel (SC) was given heat by an electric heater and kept at a constant temperature.

After that, the hydrogen gas was gradually released by the PCT program control. In case the sample could still absorb hydrogen when the pressure was increased, the PCT program added additional hydrogen gas into the system until the pressure became stable. That means the sample was saturated. The hydrogen absorption capacity (H/M ratio) would be determined from the total pressure change (Kim et al., 1999; Tominaga et al., 2015).

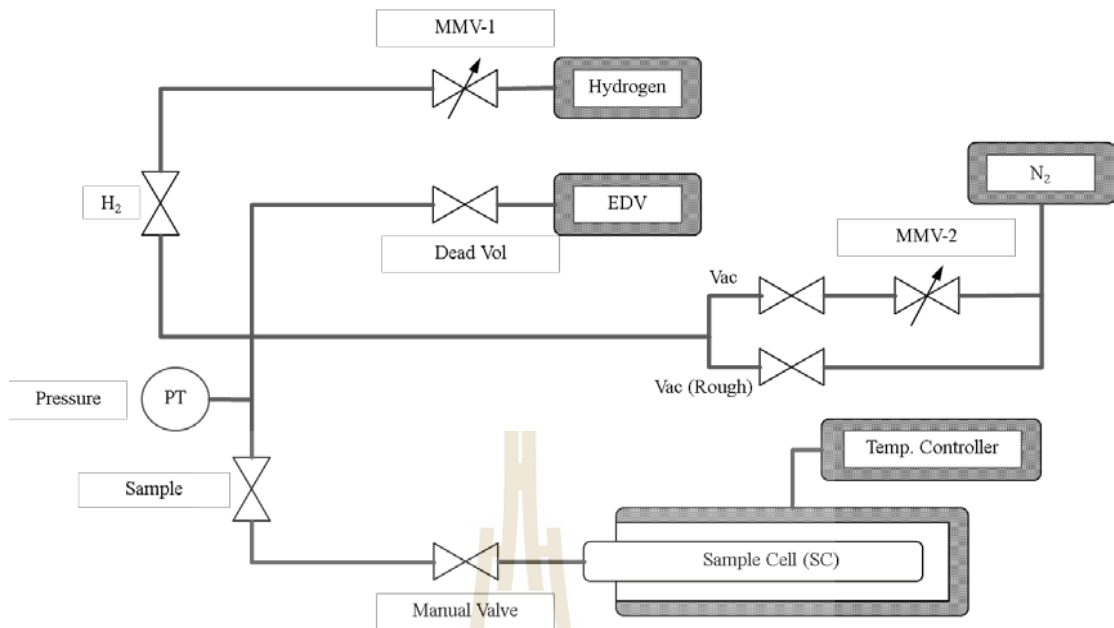


**Figure 2.15** Schematic of the PCT Sieverts' apparatus. PT, PCT pressure gauge; EDV, PCT measuring section empty cell; SC, Sample cell; MMV-1 and MMV-2, Flow regulating valves; H<sub>2</sub>, Hydrogen valve<sup>a</sup>; Sample, Sample valve<sup>a</sup>, Vac<sup>a</sup> and Vac (Rough)<sup>a</sup>.

a: Remote PCT operation valves.

## CHAPTER III

### MATERIALS AND METHODS

#### 3.1 Materials

Commercially pure powders Ti (99.9%), Zr (99.9%), Ni (99.9%), and Mg (99.9%) elemental powders are used as starting materials for mixing with the composition of the compound,  $Ti_{45-x}Zr_{38}Ni_{17}Mg_x$  ( $x=2, 4$ ). A Mixture of the sample by the mechanical alloying (MA) process in a planetary ball mill machine (Fritsch Pulverisette-7). The elemental powders were poured into the stainless-steel chamber with five stainless-steel balls (diameter of 15 mm). The weight of powder was 10.383 g. The weight of the ball to powder ratio was 8:1. A suitable for intermediate ball-milling conditions is medium milling energy (Zaluska et al., 1999; Takasaki and Kelton, 2006). The operations were performed under argon atmosphere and the samples were mechanically alloyed. The weight of each powder could be calculated as follows.

##### 3.1.1 Parameters for calculation

- a) The Composition of the compound was  $Ti_{45-x}Zr_{38}Ni_{17}Mg_x$  ( $x=2, 4$ )
- b) The atomic weight, which we know from the list of a chemical element.
- c) Total atomic weight ( $\sum$ Atomic weight)
- d) The weight of the balls
- e) The sample to Balls ratio (1:8)

### 3.1.2 The total atomic weight of $\text{Ti}_{43}\text{Zr}_{38}\text{Ni}_{17}\text{Mg}_2$

The total atomic weight was calculated from the compositions of the  $\text{Ti}_{43}\text{Zr}_{38}\text{Ni}_{17}\text{Mg}_2$  compound and the atomic weight of each element calculate as follows in Table 3.1.

**Table 3.1** Calculation of the total atomic weight of  $\text{Ti}_{43}\text{Zr}_{38}\text{Ni}_{17}\text{Mg}_2$

Elements	Compositions (a)	Atomic weight (b)	Compositions atomic weight (a x b)
Titanium (Ti)	43	47.867	<b>2058.281</b>
Zirconium (Zr)	38	91.224	<b>3466.512</b>
Nickel (Ni)	17	58.693	<b>997.781</b>
Magnesium (Mg)	2	24.304	<b>48.608</b>
Total atomic weight (c)			<b>6571.182</b>

### 3.1.3 The total sample weight of $\text{Ti}_{43}\text{Zr}_{38}\text{Ni}_{17}\text{Mg}_2$

The mass of mixed powder was calculated from a ball-to-powder ratio of 8:1. The suitable condition for intermediate ball-milling was medium milling energy (Zaluska et al., 1999; Takasaki and Kelton, 2006). The total sample weight was 10.383 g as shown in Table 3.2.

**Table 3.2** Calculation of the total sample weight (g) of  $\text{Ti}_{43}\text{Zr}_{38}\text{Ni}_{17}\text{Mg}_2$

Parameters	Sample	Ball
Ratio	1	8
Total sample: balls weight	<b>10.383 g</b>	83.064 g (from scale)

### 3.1.4 The Amount of weight of each powder of $Ti_{43}Zr_{38}Ni_{17}Mg_2$

The total weight of powder was 10.383 g which consisted of Ti (3.253 g), Zr (5.478 g), Ni (1.576 g), and Mg (0.076 g). The weight of each powder would be determined from the compositions of atomic weight and Total atomic weight as shown in Table 3.3.

**Table 3.3** Calculation of the weight of each element of the  $Ti_{43}Zr_{38}Ni_{17}Mg_2$  compound

Elements	Compositions	Compositions atomic weight	Weight (g)
Titanium	43	2058.281	<b>3.253</b>
Zirconium	38	3466.512	<b>5.478</b>
Nickel	17	997.781	<b>1.576</b>
Magnesium	2	48.608	<b>0.076</b>
	Total atomic weight	6571.182 g	<b>10.383 g</b>

### 3.2 Sample preparations

After calculating the weight of each element, the samples were mixed by mechanical alloying under two conditions (1) rotation speed 600 rpm with 20 h milling time (Tominaga et al., 2015) and (2) rotation speed 630 rpm with 30 h milling time (Azuha et al., 2020), as shown in Table 3.4.

**Table 3.4** Materials Composition and Parameters

Compositions		Parameters	
		Speed (rpm)	Milling time (hour)
a	Ti <sub>43</sub> Zr <sub>38</sub> Ni <sub>17</sub> Mg <sub>2</sub>	600	20
b	Ti <sub>43</sub> Zr <sub>38</sub> Ni <sub>17</sub> Mg <sub>2</sub>	630	30
c	Ti <sub>41</sub> Zr <sub>38</sub> Ni <sub>17</sub> Mg <sub>4</sub>	600	20
d	Ti <sub>41</sub> Zr <sub>38</sub> Ni <sub>17</sub> Mg <sub>4</sub>	630	30

After the MA process, the samples had not, yet, been transformed into instant quasicrystals. The samples needed to be annealed at annealing temperature, for a period of 2 h in a high vacuum of  $\geq 1.00 \times 10^{-4}$  Pa by a turbo molecular pump (Azuha et al., 2020). Then, the samples became amorphous phase and turned into icosahedral quasicrystal phase (i-phase) as expected. (Takasaki et al., 2002; Takasaki and Kelton, 2006).

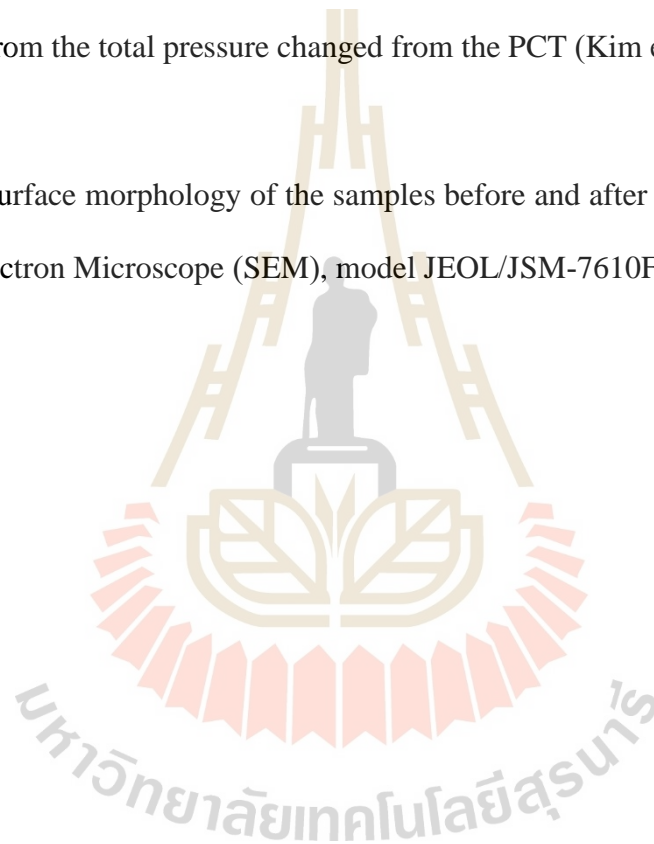
The structures of samples before and after the annealing process were analyzed and measured using Rigaku SmartLab with Cu-K $\alpha$  radiation at 30 kV and 40 mA. Previously, the sample could be transformed into i-phase after the annealing process. The annealing temperature was achieved from Differential scanning calorimetry (DSC) measurements. DSC measurements were carried out between room temperature and desired temperature using a scan rate of 5 °C min<sup>-1</sup> under an argon atmosphere.

### 3.3 The hydrogen absorption and desorption

The samples, after had gone through the annealing process, were analyzed and observed whether there was an appearance of quasicrystals. The samples, then, were hydrogenated by pressure-composition isotherms (PCT) techniques. The hydrogen-free

sample was poured into the vessel, heated by an electric heater, and kept constant at 573 K (Takasaki and Kelton, 2006). After that, the hydrogen gas was gradually released by the PCT program control. If the sample could absorb hydrogen gas while the pressure increases, that means the sample had the efficacy to absorb more hydrogen gas. The PCT will drop the pressure, and additional hydrogen will be loaded until the pressure become stable. The hydrogen absorption capacity (H/M ratio) could be determined from the total pressure changed from the PCT (Kim et al., 1999; Tominaga et al., 2015).

The surface morphology of the samples before and after PCT was observed by Scanning Electron Microscope (SEM), model JEOL/JSM-7610F (Azuha et al., 2020).



## CHAPTER IV

### RESULTS AND DISCUSSION

#### 4.1 Analysis to identify the appearing i-phase of $\text{Ti}_{45-x}\text{Zr}_{38}\text{Ni}_{17}\text{Mg}_x$ , ( $x=2, 4$ ) compound

The X-ray diffraction (XRD) patterns of  $\text{Ti}_{45-x}\text{Zr}_{38}\text{Ni}_{17}\text{Mg}_x$ , ( $x=2, 4$ ) before the MA process follow the conditions in table 3.4. They appeared, overall, to be the amorphous phase observed in all compositions and conditions. However, if we consider in the range  $2\theta$  of 30-35 deg. There was a tiny peak of the Magnesium-Zirconium Alloy (Mg-Zr) phase shown in Figure 4.1. The results were in accordance with the previous works, which suggested that the amorphous phase could not be found right after the MA process. However, the amorphous phase could be transformed into i-phase after the samples were annealed at 2 h (Takasaki and Kelton, 2006).

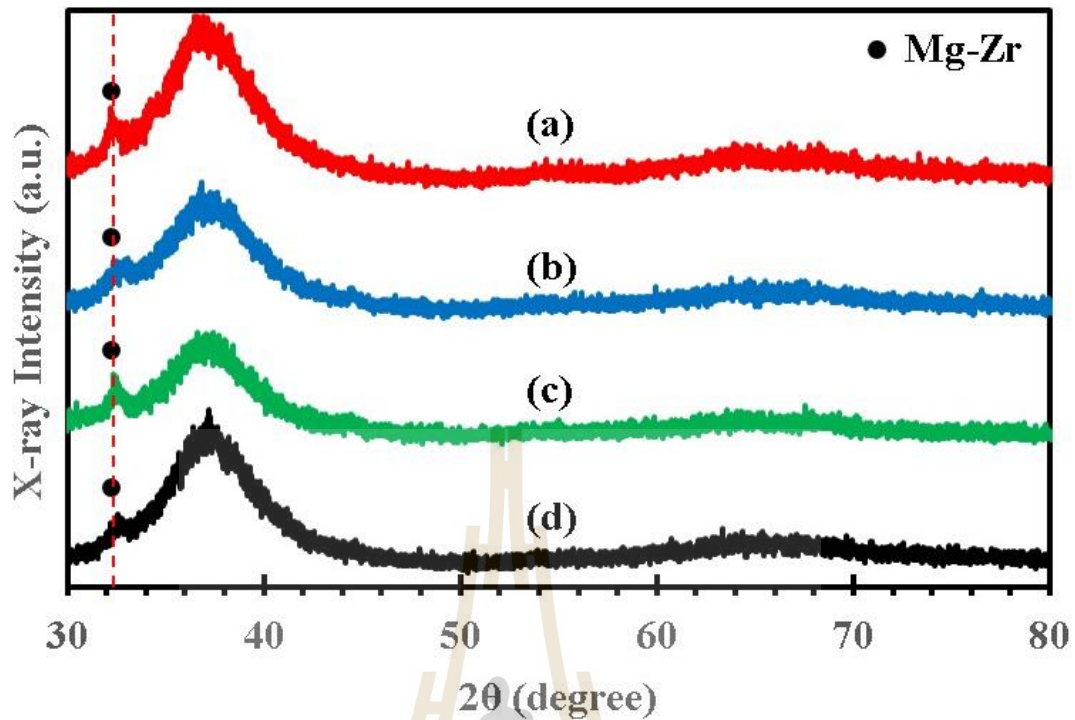
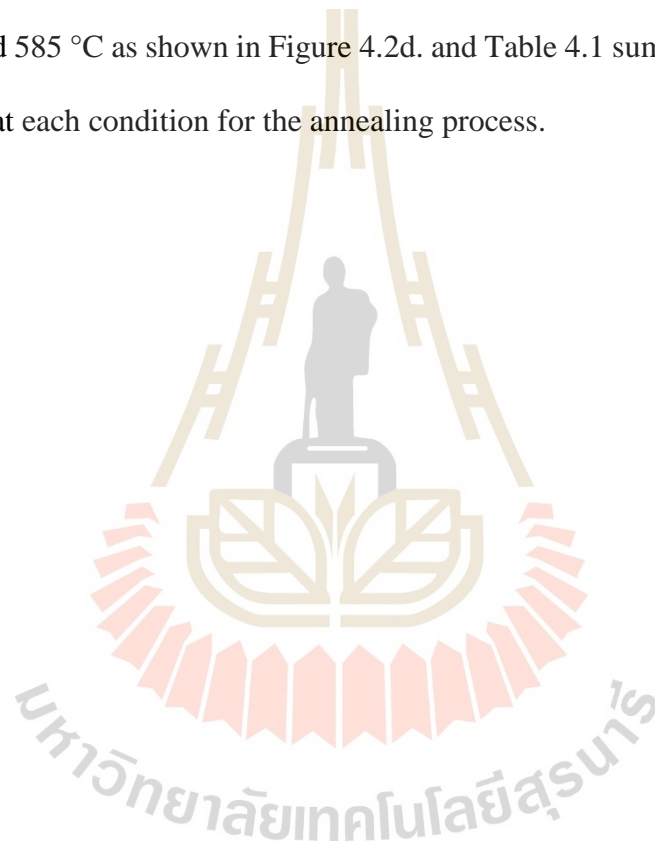


**Figure 4.1** The X-ray diffraction patterns of  $\text{Ti}_{45-x}\text{Zr}_{38}\text{Ni}_{17}\text{Mg}_x$ , ( $x=2, 4$ ) compounds after the mechanical alloying process

- (a)  $\text{Ti}_{43}\text{Zr}_{38}\text{Ni}_{17}\text{Mg}_2$  Rotation speed 600 rpm, time 20 h
- (b)  $\text{Ti}_{43}\text{Zr}_{38}\text{Ni}_{17}\text{Mg}_2$  Rotation speed 630 rpm, time 30 h
- (c)  $\text{Ti}_{41}\text{Zr}_{38}\text{Ni}_{17}\text{Mg}_4$  Rotation speed 600 rpm, time 20 h
- (d)  $\text{Ti}_{41}\text{Zr}_{38}\text{Ni}_{17}\text{Mg}_4$  Rotation speed 630 rpm, time 30 h

The samples were mechanically alloyed by the ball mill process. As described earlier, the annealing temperature could be obtained from the onset-temperature of the Differential scanning calorimetry (DSC) results because the onset- temperature should suffer unchanged when peak-temperature shifted due to heating rate and sample mass (Floriano et al., 2012; Fucke et al., 2010). Figure 4.2 shows the DSC curve. It shows that the composition of the  $\text{Ti}_{43}\text{Zr}_{38}\text{Ni}_{17}\text{Mg}_2$  compound with a rotation speed of 600 rpm with time 20 h exhibited the onset temperature of the crystallization at 550 °C as

shown in Figure 4.2a. At the same time, the  $\text{Ti}_{43}\text{Zr}_{38}\text{Ni}_{17}\text{Mg}_2$  compound with a rotation speed of 630 rpm with time 30 h was observed to have a temperature of 500 °C as shown in Figure 4.2b. The  $\text{Ti}_{41}\text{Zr}_{38}\text{Ni}_{17}\text{Mg}_4$  compound with a rotation speed of 600 rpm with time 20 h of was observed to have a temperature of 576 °C as shown in Figure 4.2c. For the  $\text{Ti}_{41}\text{Zr}_{38}\text{Ni}_{17}\text{Mg}_4$  compound with the rotation speed of 630 rpm with time 30 h, there appeared, on the chart, two peaks, and was observed to have temperatures of 575 °C and 585 °C as shown in Figure 4.2d. and Table 4.1 summarized the observed temperature at each condition for the annealing process.



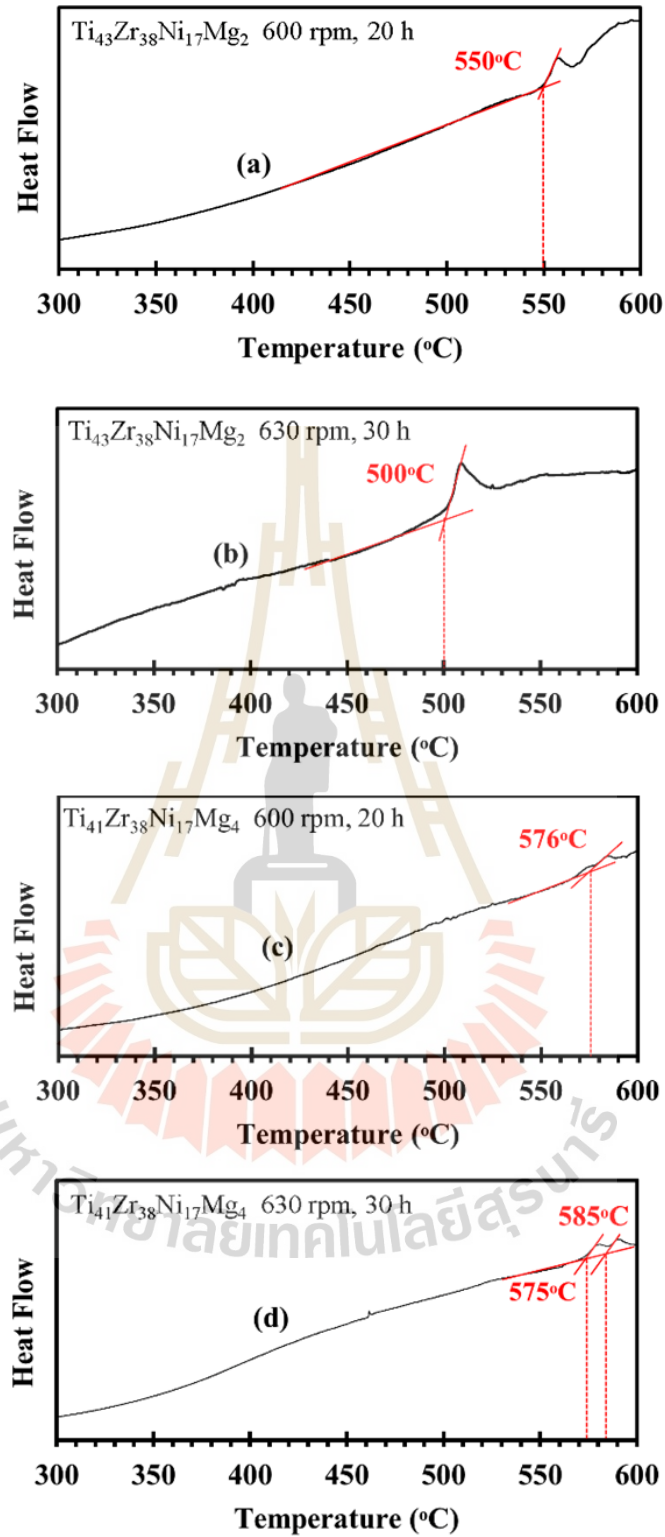


**Figure 4.2** Differential scanning calorimetry of  $\text{Ti}_{45-x}\text{Zr}_{38}\text{Ni}_{17}\text{Mg}_x$ , ( $x=2, 4$ )

compounds after the mechanical alloying process

- (a)  $\text{Ti}_{43}\text{Zr}_{38}\text{Ni}_{17}\text{Mg}_2$  at 600 rpm 20 h
- (b)  $\text{Ti}_{43}\text{Zr}_{38}\text{Ni}_{17}\text{Mg}_2$  at 630 rpm 30 h
- (c)  $\text{Ti}_{41}\text{Zr}_{38}\text{Ni}_{17}\text{Mg}_4$  at 600 rpm 20 h
- (d)  $\text{Ti}_{41}\text{Zr}_{38}\text{Ni}_{17}\text{Mg}_4$  at 630 rpm 30 h

**Table 4.1** The annealing temperature obtained from Differential scanning calorimetry (DSC) analysis of  $\text{Ti}_{45-x}\text{Zr}_{38}\text{Ni}_{17}\text{Mg}_x$ , ( $x=2, 4$ ) compounds

Composition	Parameters		Annealing Temperature (°C)
	Speed (rpm)	Milling time (h)	
a $\text{Ti}_{43}\text{Zr}_{38}\text{Ni}_{17}\text{Mg}_2$	600	20	550
b $\text{Ti}_{43}\text{Zr}_{38}\text{Ni}_{17}\text{Mg}_2$	630	30	500
c $\text{Ti}_{41}\text{Zr}_{38}\text{Ni}_{17}\text{Mg}_4$	600	20	576
d $\text{Ti}_{41}\text{Zr}_{38}\text{Ni}_{17}\text{Mg}_4$	630	30	585
e $\text{Ti}_{41}\text{Zr}_{38}\text{Ni}_{17}\text{Mg}_4$	630	30	575

Figure 4.4 shows the XRD patterns of  $\text{Ti}_{45-x}\text{Zr}_{38}\text{Ni}_{17}\text{Mg}_x$ , ( $x=2, 4$ ) compounds after the annealing process for a period of 2 h (Takasaki et al., 2002; Takasaki and Kelton, 2006). It shows that the quasicrystal has appeared in almost all conditions and compositions. Similar results were also found in the previous work conducted by Takasaki and Kelton., (2006). For the compound  $\text{Ti}_{41}\text{Zr}_{38}\text{Ni}_{17}\text{Mg}_4$  with the rotation speed 630 rpm, with 30 hours milling time, at an annealing temperature of 575 °C, it could not be transformed into i-phase like other conditions (Figure 4.4e). However, if

we consider another peak of the DSC curve, we know that at the temperature of 585 °C, it could be transformed into i-phase (Figure 4.4d).

Although the amount of the i-phase has appeared at angle 2 thetas of 35-44 degrees, 65 degrees, and 76-78 degrees in all conditions and compositions (Figure 4.4a-4.4d), it does not occur with the rotation speed of 630 rpm with 30 hours milling time of  $\text{Ti}_{43}\text{Zr}_{38}\text{Ni}_{17}\text{Mg}_2$ . If we exclusively look at angle 2 thetas of 44 degrees and 76-78 degrees, two types of crystal phases including  $\text{Ti}_2\text{Ni}$  and  $\text{Mg}_2\text{Ni}$  were reported to have the ability to store hydrogen.

From Figure 4.4a-4.4b, in the  $\text{Ti}_{43}\text{Zr}_{38}\text{Ni}_{17}\text{Mg}_2$  compound at rotation speed 600 rpm with 20 hours milling time and in  $\text{Ti}_{41}\text{Zr}_{38}\text{Ni}_{17}\text{Mg}_4$  compound at both same conditions, only  $\text{Mg}_2\text{Ni}$  could be found at angle 2 thetas of 44 degrees. However, at 66 degrees, there appear both crystal phase ( $\text{Ti}_2\text{Ni}$  and  $\text{Mg}_2\text{Ni}$ ).

On the other hand, in the  $\text{Ti}_{43}\text{Zr}_{38}\text{Ni}_{17}\text{Mg}_2$  compound at a rotation speed of 630 rpm with 30 hours milling time, both crystal phase ( $\text{Ti}_2\text{Ni}$  and  $\text{Mg}_2\text{Ni}$ ) has appeared at angle 2 thetas of 40-45 degrees, but at 66 degrees, only  $\text{Mg}_2\text{Ni}$  has appeared. However, in all conditions and composition (a-d) an equal amount of crystal-phases was found.

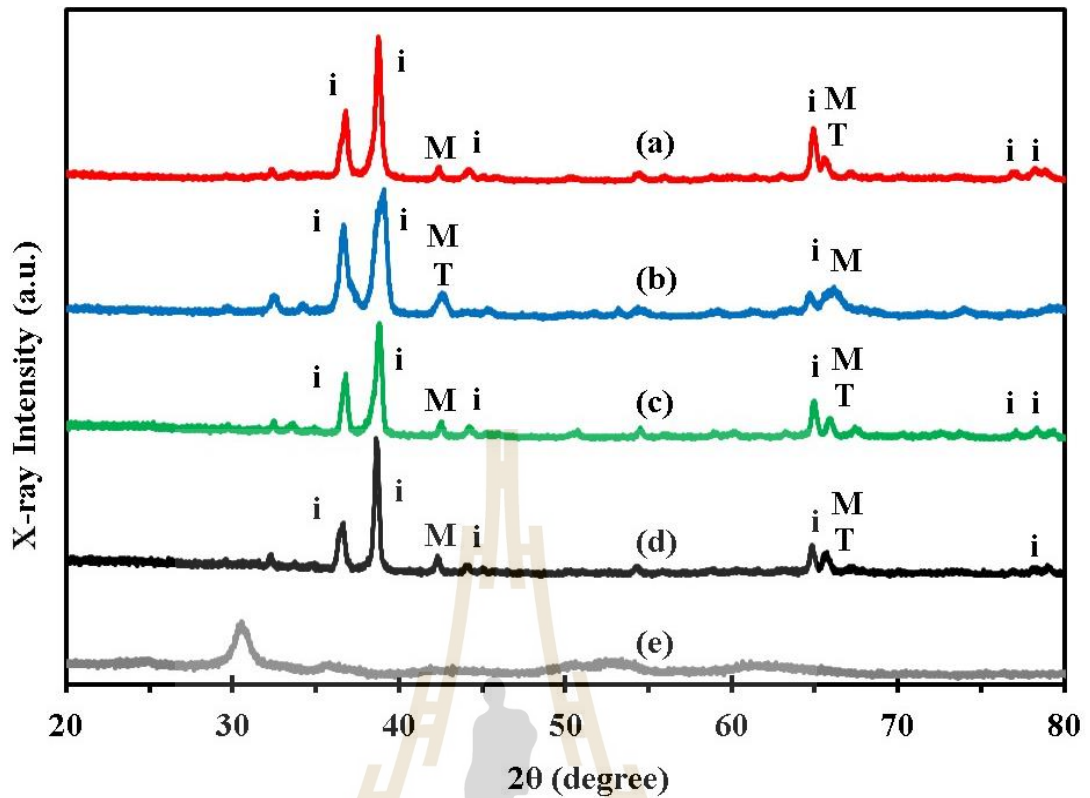


**Figure 4.3** The X-ray diffraction patterns  $\text{Ti}_{45-x}\text{Zr}_{38}\text{Ni}_{17}\text{Mg}_x$ , ( $x=2, 4$ ) compounds after annealing ( $i$  = i-phase,  $M$  =  $\text{Mg}_2\text{Ni}$ ,  $T$  =  $\text{Ti}_2\text{Ni}$ )

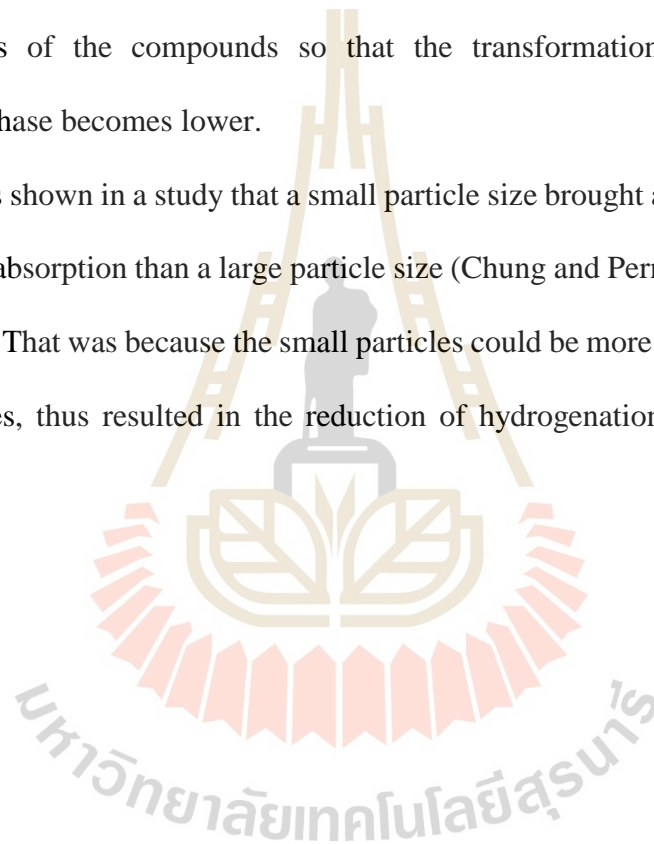
- (a)  $\text{Ti}_{43}\text{Zr}_{38}\text{Ni}_{17}\text{Mg}_2$  speed 600 rpm, time 20 h with Temp. 550 °C
- (b)  $\text{Ti}_{43}\text{Zr}_{38}\text{Ni}_{17}\text{Mg}_2$  speed 630 rpm, time 30 h with Temp. 500 °C
- (c)  $\text{Ti}_{43}\text{Zr}_{38}\text{Ni}_{17}\text{Mg}_2$  speed 600 rpm, time 20 h with Temp. 576 °C
- (b)  $\text{Ti}_{43}\text{Zr}_{38}\text{Ni}_{17}\text{Mg}_2$  speed 630 rpm, time 30 h with Temp. 585 °C
- (e)  $\text{Ti}_{43}\text{Zr}_{38}\text{Ni}_{17}\text{Mg}_2$  speed 630 rpm, time 30 h with Temp. 575 °C

Therefore, when exclusively looking at the i-phase amount, the  $\text{Ti}_{43}\text{Zr}_{38}\text{Ni}_{17}\text{Mg}_2$  compound and  $\text{Ti}_{41}\text{Zr}_{38}\text{Ni}_{17}\text{Mg}_4$  compound at rotation speed 600 rpm with 20 hours of milling time have a higher amount than other compounds. However, this work aims to study the capacity of hydrogen storage of the  $\text{Ti}_{43}\text{Zr}_{38}\text{Ni}_{17}\text{Mg}_2$  compound. Therefore, the  $\text{Ti}_{43}\text{Zr}_{38}\text{Ni}_{17}\text{Mg}_2$  compound with a rotation speed of 600 rpm with 20-hour milling

time and that with a rotation speed of 630 rpm with 30-hour milling time would be considered in the next process.

Figure 4.3 shows the morphology of the particle. The condition1 (average particle of size 46.77  $\mu\text{m}$ ) was generally larger than that of the condition 2 (average particle of size 38.75  $\mu\text{m}$ ). It could be the higher rotational speed and the longer time that caused the differences of both particle size, and the powders might yield smaller particle sizes of the compounds so that the transformation temperature of the amorphous phase becomes lower.

It was shown in a study that a small particle size brought about the lesser ability of hydrogen absorption than a large particle size (Chung and Perng, 2003; Rongeat and Roué, 2004). That was because the small particles could be more stable with oxide than large particles, thus resulted in the reduction of hydrogenation rate (Zaluska et al., 1999).



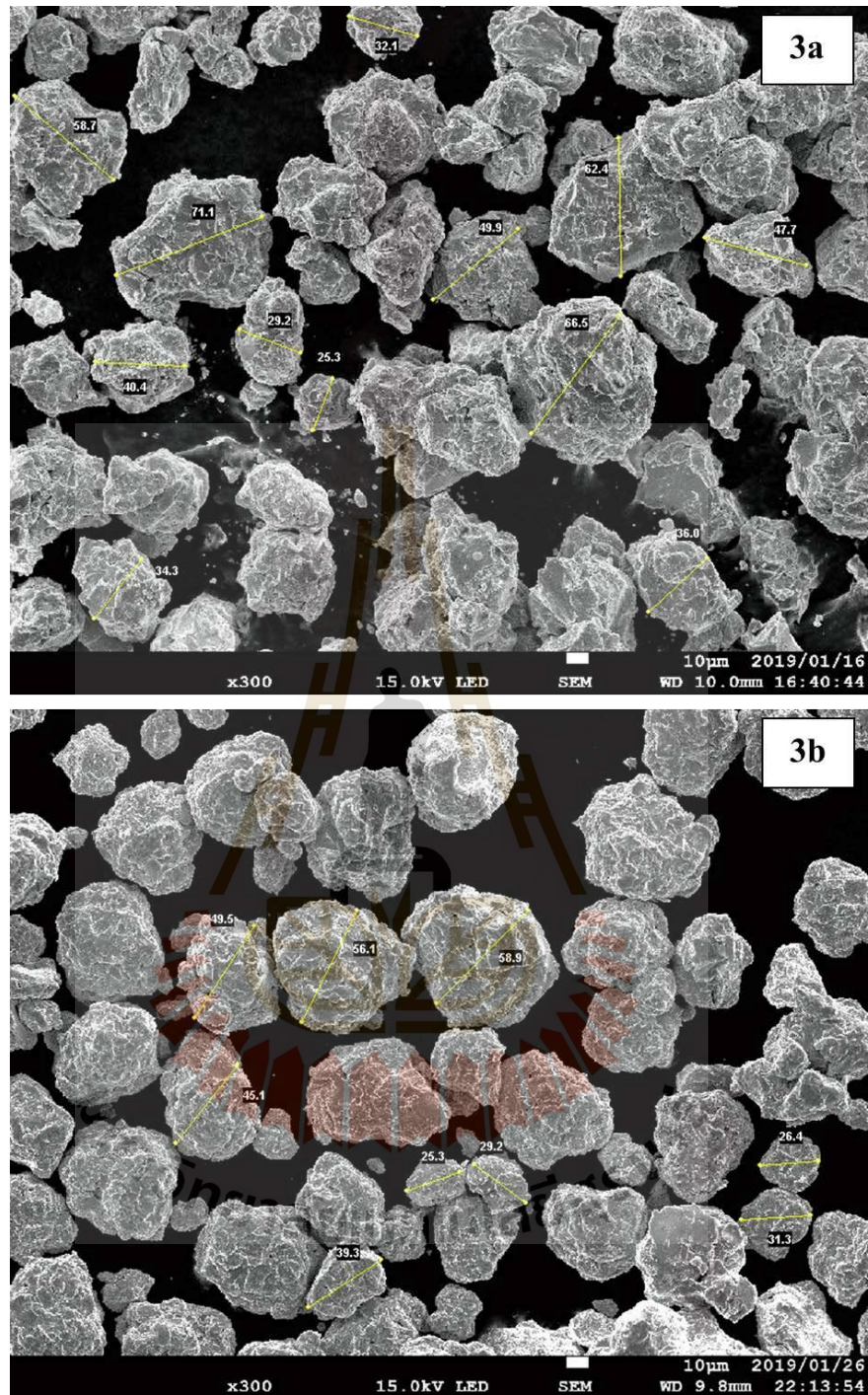


**Figure 4.4** Particles of size by SEM measurements

(4.3a)  $\text{Ti}_{43}\text{Zr}_{38}\text{Ni}_{17}\text{Mg}_2$  compound with 600 rpm with 20 h milling time

(4.3b)  $\text{Ti}_{43}\text{Zr}_{38}\text{Ni}_{17}\text{Mg}_2$  compound with 630 rpm with 30 h milling time

## 4.2 Analysis of the ability of hydrogen storage

After the samples were annealed, then came the analyzation to verify the appearance of i-phase in the  $\text{Ti}_{43}\text{Zr}_{38}\text{Ni}_{17}\text{Mg}_2$  compound. The samples were brought into the hydrogen absorption and desorption process by PCT at the temperature of 573 K. Figure 4.5 shows the hydrogen to a metal ratio (H/M) of  $\text{Ti}_{43}\text{Zr}_{38}\text{Ni}_{17}\text{Mg}_2$  compound. The maximum H/M ratio was about 1.99 with 600 rpm with 20 h milling time (condition 1). From the observation, it is higher than the H/M ratio of 1.58 for the  $\text{Ti}_{43}\text{Zr}_{38}\text{Ni}_{17}\text{Mg}_2$  compound with 630 rpm with 30 h milling time (condition 2). The hydrogen to metal (H/M) ratio could be achieved by the following equation, reported by Viano et al. (2010).

$$\frac{H}{M} = \frac{a_q^H - a_q^0}{0.1974} \quad (1)$$

The  $a_q^H$  parameter is a quasi-lattice at the hydrogen concentration of interest and  $a_q^0$  represents the measured quasi-lattice parameter for the non-hydrogenated i-phase. The value 0.1974 was measured from a slope of the quasi-lattice that expands linearly with hydrogen concentration.

Another important evidence that could identify the ability of hydrogen absorption was the lattice expansion by Deriving Bragg's Law. The law was used to explain the interference pattern of X-rays scattered by crystals could be obtained by the following equation.

$$n\lambda = 2d\sin\theta \quad (2)$$

From the equation,  $n$  is a parameter of integer,  $\lambda$  is the wavelength of the x-rays,  $d$  is the spacing between planes in the atomic lattice of the sample and  $\theta$  is the diffraction angle in degrees (Elton and Jackson, 1966).

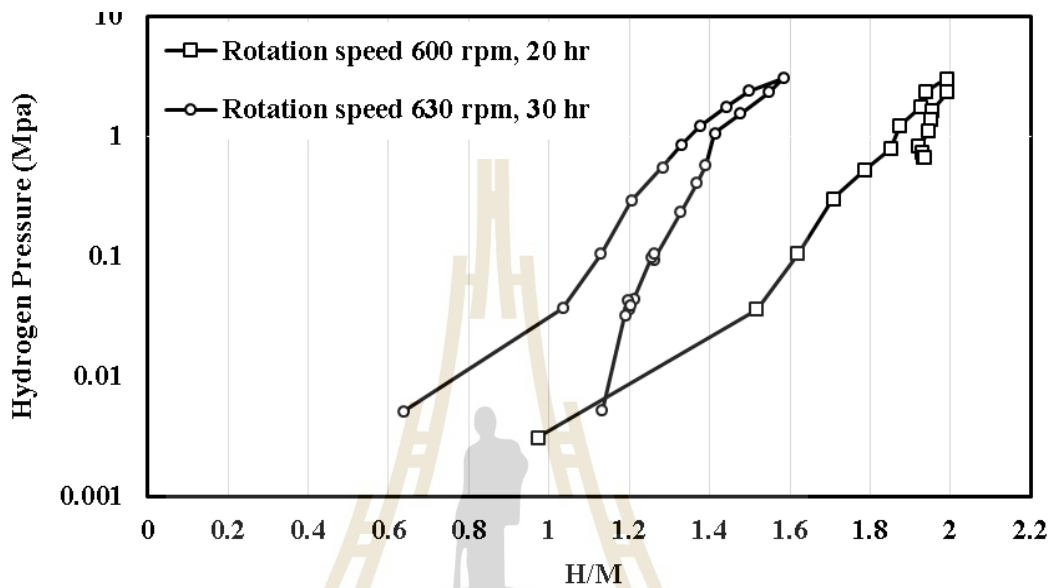


**Figure 4.5** Hydrogen absorption and desorption pressure-composition

Figure 4.6 showed the X-ray patterns of the sample after hydrogenation. This could explain the lattice expansion by considering the position of the high peaks of  $i$ -phase (110000i) in figure 4.6b (before hydrogenation) and figure. 4.6c (after hydrogenation). It was observed that the position of  $i$ -phase (110000i) shifted after hydrogenation because the space between planes in the atomic lattice of the sample was expanded.

If we compare the lattice parameter of spacing and the planes in the atomic lattice of the sample, then we can see the expansion of the lattice after hydrogenation approximately 5.87% for the MA condition 1 of 600 rpm with 20 hours. It was larger than the expansion of the lattice for MA condition 2 of 630 rpm with 30 hours whose

expansion of the lattice was approximately 3.00%. Similar results were also found in the work of Takasaki and Kelton, 2006.

The condition of 600 rpm with 20 hours lattice was expanded higher than the condition 2 of 630 rpm and 30 hours. Therefore, both results of the hydrogen to a metal ratio (H/M) of  $\text{Ti}_{43}\text{Zr}_{38}\text{Ni}_{17}\text{Mg}_2$  shown in Figure 4.5 and the lattice expansion shown in Figure 4.6 provided evidence that conditions 1 of rotations speed 600 rpm with 20 hours could absorb more hydrogen than that condition 2 of rotations speed 630 rpm with 30 hours.



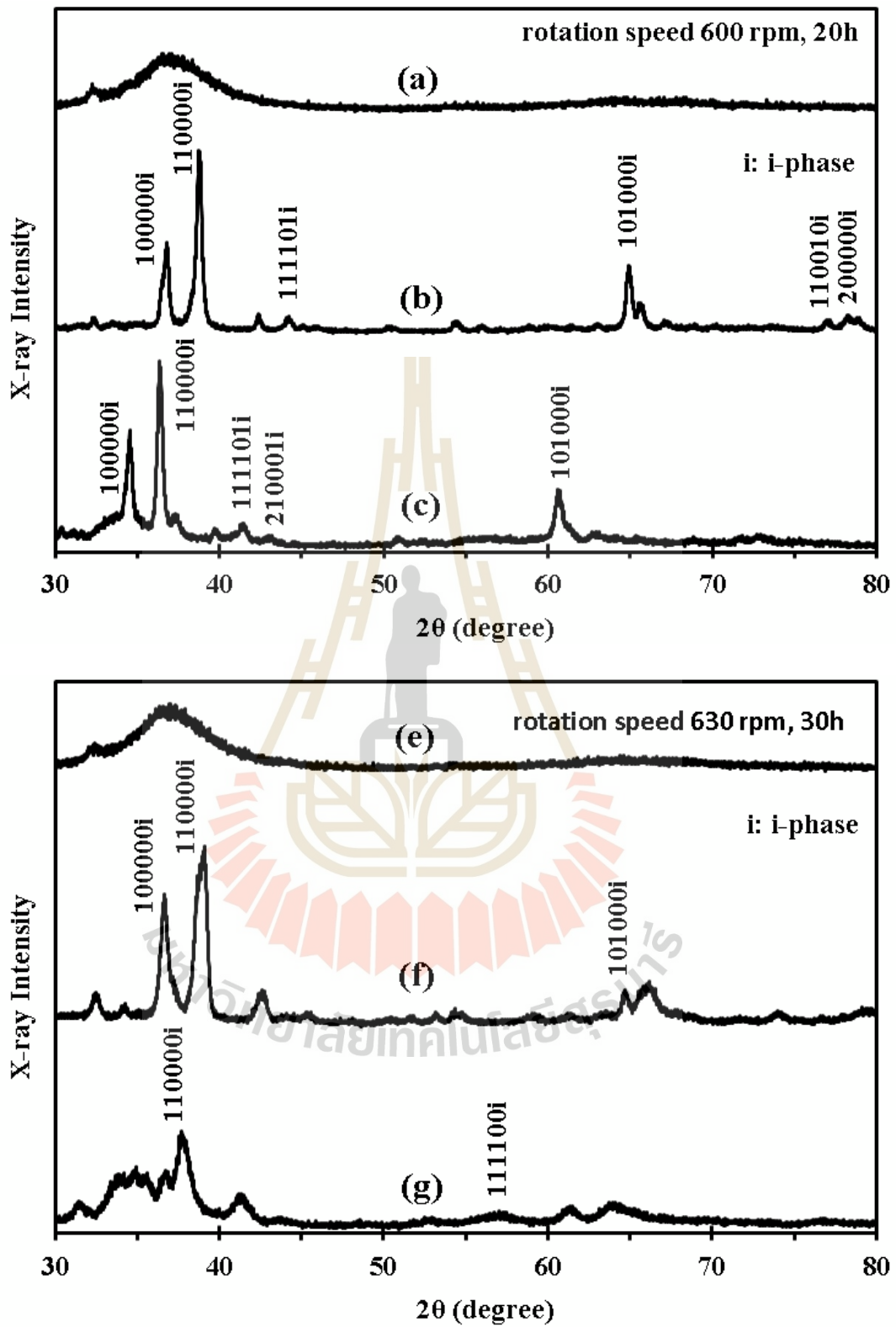


**Figure 4.6** X-ray diffraction patterns for the i-phase powder, Rotation speed 600 rpm, 20 h

(4.6a) before annealing process

(4.6b) after the annealing process

(4.6c) after pressure- composition isotherm (PCT) measurements at 573 K and rotation speed 630 rpm, 30 h

(4.6e) before annealing process

(4.6f) after the annealing process

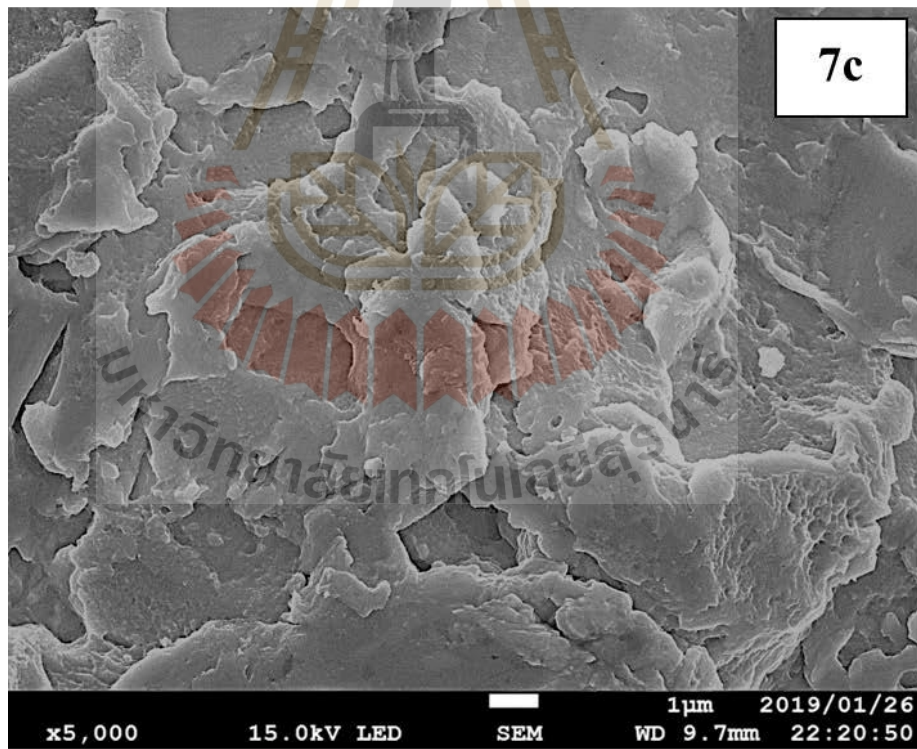
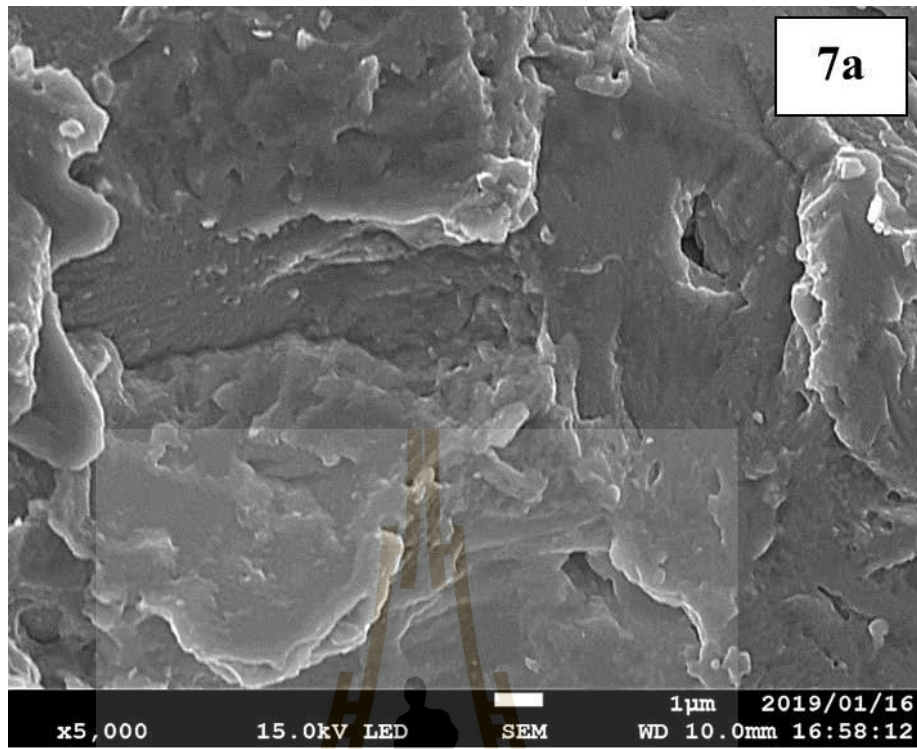
(4.6g) after pressure- composition isotherm (PCT) measurements at 573 K

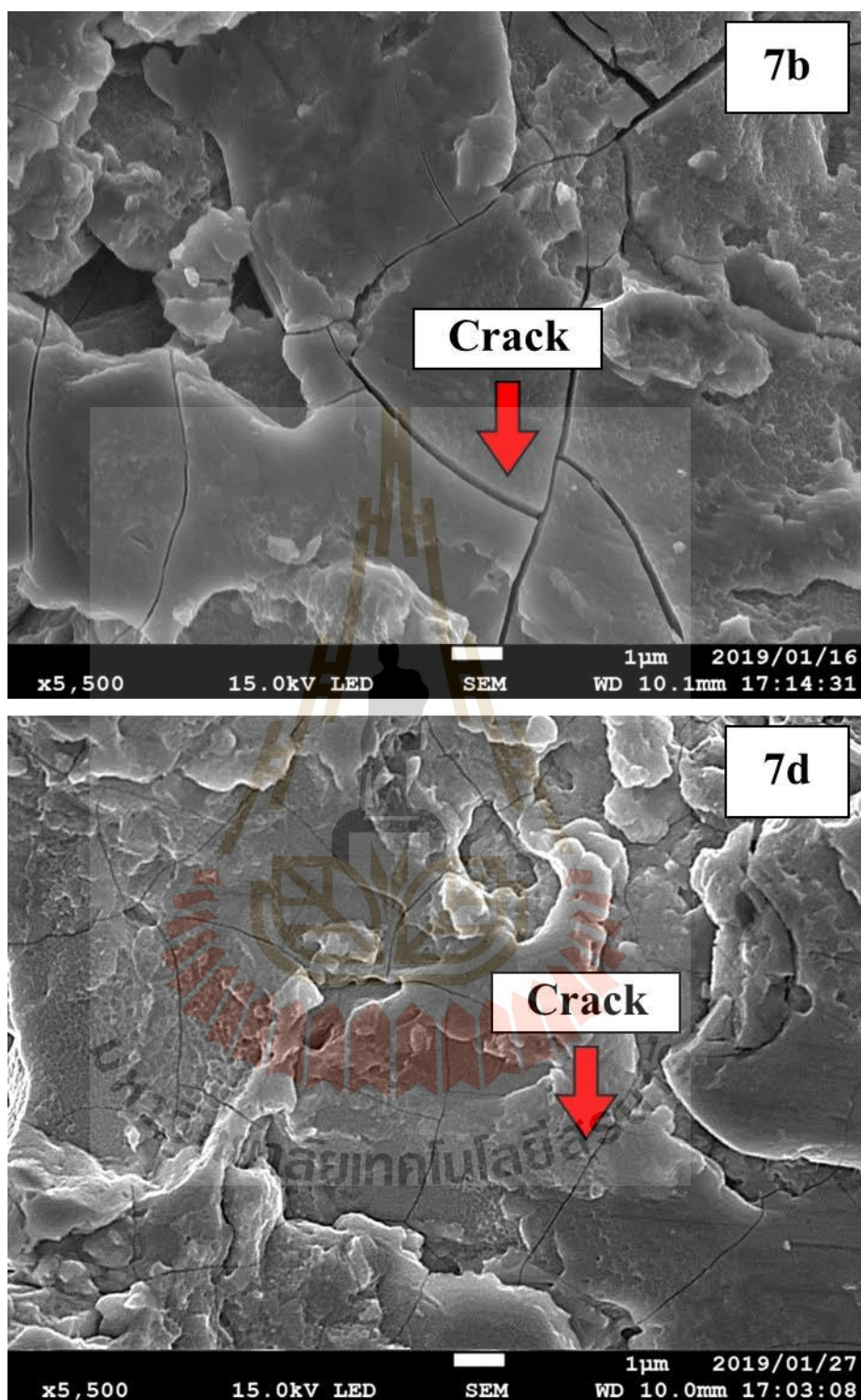
The expansion of the lattice after hydrogenation was a result of the insertion of hydrogen into the lattice of a compound. The outcome agrees with the evidence as described by SEM results in Figure 4.7.

Figure 4.7 exhibited the morphology before and after hydrogenation of the samples. If we compare Figures 4.7a and Figure 4.7b of conditions 1 (600 rpm and 20 hours) and Figure 7c and Figure 4.7d of conditions 2 (630 rpm and 30 hours), it can be seen that cracks have appeared on the surface of both conditions of  $\text{Ti}_{43}\text{Zr}_{38}\text{Ni}_{17}\text{Mg}_2$  compound after hydrogenation. The cracks have appeared perhaps because of the lattice volumetric expansion (Balcerzak et al., 2015; Diego et al., 2008).

Figure 4.7b shows the morphology after hydrogenation. In conditions 1 of 600 rpm and 20 hours, there are larger and deeper cracks than those on the sample of conditions 2 of 630 rpm and 30 hours as indicated in Figure 4.7d. These results provided evidence that the sample with larger and deeper cracks has lattice volumetric expansion more than those with smaller and shallower ones.

Therefore, this is evidence to support that if the value of the H/M ratio gets higher, the expansion also gets higher as well.





**Figure 4.7** Result of SEM analysis to compare the surface morphology of compounds before and after the hydrogenation process.

(4.7a) before hydrogenation of  $\text{Ti}_{43}\text{Zr}_{38}\text{Ni}_{17}\text{Mg}_2$  Rotation speed 600 rpm, 20 h

(4.7b) after hydrogenation of  $\text{Ti}_{43}\text{Zr}_{38}\text{Ni}_{17}\text{Mg}_2$  Rotation speed 600 rpm, 20 h

(4.7c) before hydrogenation of  $\text{Ti}_{43}\text{Zr}_{38}\text{Ni}_{17}\text{Mg}_2$  Rotation speed 630 rpm, 30 h

(4.7d) after hydrogenation of  $\text{Ti}_{43}\text{Zr}_{38}\text{Ni}_{17}\text{Mg}_2$  Rotation speed 630 rpm, 30 h

### 4.3 Crystals phase

Adding the Mg into the Ti-Zr-Ni quasicrystal could be one of the causes that increased the hydrogen-storing ability due to Mg is a primary material that has the potential to absorb hydrogen. It is reported that Ti-Ni alloy ( $\text{Ti}_2\text{Ni}$ ) has hydrogen storage ability up to 0.83 H/M, Nobuki, et al., (2019), and Ti-Ni-Mg alloy could raise H/M ratio to 1.6, Mori et al., (2007). It was implied that Mg might play an important role in enhancing hydrogen absorbability. Therefore, from the hypothesis above, it can be said that the higher hydrogen storage capacity is a result of magnesium doping into the Ti-based alloy with the appropriated mechanical alloying condition as shown in Table 4.2.

**Table 4.2** Estimated the hydrogen to metal atom (H/M) ratio with that of the other Ti-based i-phases.

Composition	Parameters		H/M	Authors
	Speed (rpm)	Milling time (h)		
$\text{Ti}_{45}\text{Zr}_{38}\text{Ni}_{17}$	600	20	1.30	Tominaga et al. (2015)
$\text{Ti}_{43}\text{Zr}_{38}\text{Ni}_{17}\text{Mg}_2$	600	20	1.99	This work
$\text{Ti}_{43}\text{Zr}_{38}\text{Ni}_{17}\text{Mg}_2$	630	30	1.58	This work

# CHAPTER V

## CONCLUSIONS

This research was undertaken to investigate the formation of icosahedral quasicrystal (i- phase) and crystal phases of mixed materials between Ti- based quasicrystals (Ti-Zr- Ni) and Magnesium (Mg) by using a mechanical alloying (MA) process. The capacity of hydrogen storage and the hydrogen-to-metal (H/M) ratio was also investigated. MA process was conducted under two conditions; (i) rotation speed of 600 rpm with 20 h milling time and (ii) rotation speed of 630 rpm with 30 h milling time. The following conclusions can be drawn from this study:

- (1) The  $\text{Ti}_{43}\text{Zr}_{38}\text{Ni}_{17}\text{Mg}_2$  compound after MA was transformed from amorphous to icosahedral and crystal phases after the annealing process.
- (2) The  $\text{Ti}_{43}\text{Zr}_{38}\text{Ni}_{17}\text{Mg}_2$  compound with 600 rpm with 20 h milling time yielded a high capacity for hydrogen storage with a hydrogen-to-metal ratio (H/M) of 1.99. This was higher than the compound with 630 rpm with 30 h milling time.
- (3) The higher capacity of hydrogen storage might be influenced by Mg doping into the Ti-Zr-Ni system with an appropriate mechanical alloying condition.

## REFERENCES

- Azuha, A. A., Klimkowicz, A., and Takasaki, A. (2020). Quaternary Quasicrystal Alloys for Hydrogen Storage Technology. **MRS Advances**. vol. 5, no. 20, pp. 1071-1083.
- Balcerzak, M., and Jurczyk M. (2015). Influence of Gaseous Activation on Hydrogen Sorption Properties of TiNi and Ti<sub>2</sub>Ni Alloys. **J. of Materials Eng. and Performance**. vol. 24, no. 4, pp. 1710-1717.
- Botta, W.J. (2012). Magnesium-Nickel Alloy for Hydrogen Storage Produced by Melt Spinning Followed by Cold Rolling. **J. of Materials Research**. pp. 813-817, 2012.
- Chung, S.-R., and Perng, T.-P. (2003). Effect of particle size on hydrogenation properties of a gas-atomized AB<sub>5</sub>-type alloy. **J. of alloys and comp.** vol. 353, no. 1-2, pp. 289-294.
- Diego, E., Srinivasan, S., Goswami, Y. and Stefanakos, E. (2008). Hydrogen storage behavior of ZrNi<sub>70/30</sub> and ZrNi<sub>30/70</sub> composites. **J. Alloy Comp.** pp. 458:223-30.
- Durbin, D.J., and Malardier-Jugroot, C. (2013). Review of hydrogen storage techniques for on board vehicle applications. **J. Hydrogen Energy**. vol. 38, no. 34, pp. 14595-14617, 2013.
- Elton, L. and Jackson, D. F. (1966). X-ray diffraction and the Bragg law. **American J. of Physics**. vol. 34, no. 11, pp. 1036-1038.

- Epp, J. (2016). X-ray diffraction (XRD) techniques for materials characterization. **Materials Characterization Using Nondestructive Evaluation (NDE) Methods**, pp. 82-124, 2016.
- Fucke K., Steed J. and Anderson k. (2010). Differential scanning calorimetry (DSC). **Engineering & Physical Sciences Research Council (EPSRC) and Durham University**. United Kingdom: Fucke K.<http://www.hydrateweb.org>. 2010
- Floriano, R., Leiva, D. R., Deledda, S., Hauback, B. C., and Botta, W. J. (2013). Nanostructured MgH<sub>2</sub> obtained by cold rolling combined with short-time high-energy ball milling. **Materials Research**, vol. 16, no. 1, pp. 158-163.
- Hosni, B. Fenineche, N., ElKedim, O., Khaldi, C., and Lamloumi, J. (2017). Structural and electrochemical properties of TiFe alloys synthesized by ball milling for hydrogen storage. **J. Solid State Electrochem**. 2017.
- Jain, I.P., Chhagan Lal, and Ankur Jain. (2010). Hydrogen storage in Mg: A most promising material. **I.J. Hydrogen Energy**, pp. 35: 5133-44.
- Jayalakshmi, S., Ahn, J.P., Kim, K.B., and Fleury, E. (2007). Hydrogen-induced amorphization and embrittlement resistance in Ti-based in situ composite with bcc-phase in an amorphous matrix. **J. of Materials Research**. Vol. 22, no. 2, pp. 428-436, 2007.
- Khadka, P., Ro, J., Kim, H., Kim, I., Kim, J.T., Kim, H., Cho, J.M., Yun, G. and Lee, J. (2014). Pharmaceutical particle technologies: An approach to improve drug solubility, dissolution and bioavailability. **J. of pharmaceutical sciences**, pp. 304-316, 2014

- Kim, J.Y., Gibbons P.C. and Kelton K.F. (1999). Hydrogenation of Pd-coated samples of the Ti–Zr-based icosahedral phase and related crystalline phases. **J. Alloys and Comp.** pp 5: 589–592.
- Leiva, D.R., Ro, J., Costa, C.A., Huot, J., Pinheiro, T.S., Jorge, A., Ishikawa, T.T., and Ueda, T. T., Tsukahara, M., Kamiya, Y., and Kikuchi, S. (2005). Preparation and hydrogen storage properties of Mg–Ni–Mg<sub>2</sub>Ni laminate composites. **J. alloys and compounds.** vol. 386, no. 1-2, pp. 253-257, 2005.
- Mori, R., Kikuchi, S., Tanaka, K., Takeichi, N., Tanaka, H., Kuriyama, N., Ueda, T. T., and Tsukahara, M. (2007). Hydrogenation characteristics of Mg based alloy prepared by super lamination technique. **Materials Science.** pp. 1609-1612.
- Morozov, A. Yu., Isaev, É I. and Vekilov, Yu. Kh. (2006). Charge state and diffusion of hydrogen in the TiZrNi icosahedral alloy. **J. Physics of the Solid state.** pp. 48: 1625-28.
- Nobuki, T., Crivello, J.-C., Cuevas, F., and Joubert, J.-M.(2019). Fast synthesis of TiNi by mechanical alloying and its hydrogenation properties. **I.J. of Hydrogen Energy.** vol. 44, no. 21, pp. 10770-10776.
- Reilly, J.J. and Wiswall, R. H. (1968). The Reaction of Hydrogen with Alloys of Magnesium and Nickel and the Formation of Mg<sub>2</sub>NiH<sub>4</sub>. **Inorganic Chemistry.** pp. 07: 2254-2256.
- Rong, C., and Shen, B. (2018). Nanocrystalline and nanocomposite permanent magnets by melt spinning technique. **Chin. Phys. B.** Vol. 27, no. 11, 2018.
- Rongeat, C., and Roué, L. (2004). Effect of particle size on the electrode performance of MgNi hydrogen storage alloy. **J. of power sources.** vol. 132, no. 1-2, pp. 302-308.

- Samavat, F., Mohammad, H.T., Habibi, S., Jaleh, B., and Parisa, T.A. (2012). Quasicrystals. **J. Phys. Chem.** pp. 02: 7-14.
- Samavat, F., Tavakoli, M. H., Habibi, S., Jaleh, B., and Ahmad, P. T. (2012) . Quasicrystals. **J. of Physical Chem.** Vol. 2, no. 1, pp. 8, 2012.
- Shahi, R.R., Yadav, T. P., Shaz, M.A., Jaleh, B., Srivastava, O.N., and van Smaalen, S. (2011) . Effect of processing parameter on hydrogen storage characteristics of as quenched  $Ti_{45}Zr_{38}Ni_{17}$  quasicrystalline alloys **J. Hydrogen Energy.** pp. 592-599, 2012.
- Suryanarayana, C. (2019). Mechanical Alloying: A Novel Technique to Synthesize Advanced Materials. **J. of cast.** pp. 17, 2019.
- Shechtman, D., Blech, I., Gratias, D. and Cahn, J.W. (1984). Metallic Phase with Long-Range Orientational Order and No Translational Symmetry. **Phys. Review Letters.** pp. 53: 1951-53.
- Takasaki, A. and Kelton, K. (2006). Hydrogen storage in Ti-based quasicrystal powders produced by mechanical alloying. **I.J. Hydrogen Energy.** pp. 31: 183-90.
- Takasaki, A., Huett, V.T. and Kelton, K.F. (2002). Hydrogenation of Ti–Zr–Ni quasicrystals synthesized by mechanical alloying. **J. Non-Crystalline Solids.** pp. 334-335: 457-60.
- Tominaga, T., Takasaki, A., Shibato, T. and Świerczek, K. (2015). HREM observation and high-pressure composition isotherm measurement of  $Ti_{45} Zr_{38} Ni_{17}$  quasicrystal powders synthesized by mechanical alloying. **J. Alloys and Comp.** pp. 645: S292-S94.

- Ueda, T. T., Tsukahara, M., Kamiya, Y., and Kikuchi, S. (2005). Preparation and hydrogen storage properties of Mg–Ni–Mg<sub>2</sub>Ni laminate composites. **J. alloys and compounds**. vol. 386, no. 1-2, pp. 253-257, 2005
- Viano, A., Majzoub, E., Stroud, R., Kramer, M., Misture, S., Gibbons, P., and Kelton, K. (1998). Hydrogen absorption and storage in quasicrystalline and related Ti–Zr–Ni alloys. **Philosophical Magazine A**. vol. 78, no. 1, pp. 131-142.
- Yang, J., Sudik, A., Wolverton, C., and Siegel, D. J. (2010). High capacity hydrogen storage materials: attributes for automotive applications and techniques for materials discovery. **Chemical Society Reviews**. vol. 39, no. 2, pp. 656-675, 2010.
- Wang, Y., and Wang Y. (2017). Recent advances in additive-enhanced magnesium hydride for hydrogen storage. **J. Materials International**. pp. 27:41-49.
- Xiangyu, Z., Liqun, M., Yao, Y., Ding, Y., and Xiaodong, S. (2010). Ti<sub>2</sub>Ni alloy: a potential candidate for hydrogen storage in nickel/metal hydride secondary batteries. **J. Energy & Environmental Science**. pp. 3: 1316-1321.
- Zaluski, L., Zaluska A. and Strom-Olsen J.O. (1995). Hydrogen absorption in nanocrystalline Mg<sub>2</sub>Ni formed by mechanical alloying. **J Alloys and Comp.** 217: 245-249.
- Zaluska, A., Zaluski, L., and Ström-Olsen, J. (1999). Synergy of hydrogen sorption in ball-milled hydrides of Mg and Mg<sub>2</sub>Ni. **J. Alloys and Comp.** vol. 289, no. 1-2, pp. 197-206.

## **BIOGRAPHY**

Nitirut Phongsirimethi was born on July 24, 1994 in Buriram Province, Thailand. Nitirut received bachelor's degree in Product Design Engineering program in from Suranaree University of Technology (SUT). In addition, Nitirut is going to finish his for master's degree in Mechanical and Process System Engineering program in September 2020.

